2007-03-10

Development of an Efficient Solar Powered Unmanned Aerial Vehicle with an Onboard Solar Tracker

Troy Dixon Tegeder
Brigham Young University - Provo

DEVELOPMENT OF AN EFFICIENT SOLAR POWERED UNMANNED AERIAL VEHICLE WITH AN ONBOARD SOLAR TRACKER

by

Troy Tegeder

A thesis submitted to the faculty of

Brigham Young University

in partial fulfillment of the requirements for the degree of

Master of Science

Department of Mechanical Engineering

Brigham Young University

April 2007

BRIGHAM YOUNG UNIVERSITY

GRADUATE COMMITTEE APPROVAL

of a thesis submitted by

Troy Tegeder

This thesis has been read by each member of the following graduate committee and by majority vote has been found to be satisfactory.

Date	W. Jerry Bowman, Chair
Date	Timothy W. McLain
Date	Deryl O. Snyder

BRIGHAM YOUNG UNIVERSITY

As chair of the candidate's graduate committee, I have read the thesis of Troy Tegeder in its final form and have found (1) its format, citations and bibliographical style are consistent and acceptable and fulfill university and department style requirements; (2) its illustrative materials including figures, tables, and charts are in place; and (3) the final manuscript is satisfactory to the graduate committee and is ready for submission to the university library.

Date	W. Jerry Bowman Chair, Graduate Committee

Accepted for the Department

Date	Matthew R. Jones Graduate Coordinator

Accepted for the College

Date	Alan R. Parkinson Dean, Ira A. Fulton College of Engineering and Technology

ABSTRACT

DEVELOPMENT OF AN EFFICIENT SOLAR POWERED UNMANNED AERIAL VEHICLE WITH AN ONBOARD SOLAR TRACKER

Troy Tegeder

Department of Mechanical Engineering

Master of Science

Methods were developed for the design of a solar powered UAV capable of tracking the sun to achieve maximum solar energy capture. A single-axis solar tracking system was designed and constructed. This system autonomously rotated an onboard solar panel to find the angle of maximum solar irradiance while the UAV was airborne. A microcontroller was programmed and implemented to control the solar tracking system. A solar panel and an efficient airframe capable of housing the solar tracking system was designed and constructed. Each of these subsystems was tested individually with either ground or flight tests. Ultimately, the final assembled system was tested. These tests were used to determine where and when a UAV with an onboard solar tracker

would be advantageous over a conventional solar powered UAV with PV cells statically fixed to its wings.

The final UAV had a wingspan of 3.2 meters, a length of 2.6 meters, and weighed 4.1 kilograms. Its solar panel provided a maximum power output of 37.7 watts. The predicted system performance, airframe drag, and system power requirements were validated with a battery powered flight test. The UAV's analytical model predicted the drag to be 41% lower than the actual drag found from flight testing. Full system functionality was verified with a solar powered flight test. The results and analysis of the system tests are presented in this thesis. The net energy increase from the solar tracking UAV over a conventional solar powered UAV for the duration of a day is dependent on season and geographical location. The solar tracking UAV that was developed was found to have a maximum net energy gain of 34.5% over a conventional solar powered version of the UAV. The minimum net energy gain of the solar tracking UAV was found to be 0.8%.

ACKNOWLEDGMENTS

I would like to acknowledge Dr. W. Jerry Bowman who has really gone above and beyond in helping me with this work. Without his guidance I likely would not have been able to choose a thesis topic that is of such a great interest to me. I would also like to acknowledge Dr. Tim McLain and Dr. Deryl Snyder for their support. I am very grateful to the Mechanical Engineering Department at Brigham Young University for use of the laboratories, and for donating some of the necessary hardware for this project. I am also grateful to Shell Solar for donating the solar cells for this project, and I would like to thank the NASA Rocky Mountain Space Grant Consortium for their help in funding some of this project. Most of all I would like to thank my wife, Nancee, who has been my inspiration in this project from start to finish.

Table of Contents

Abstract . . . . . **iv**

Acknowledgments . . . . . **vi**

List of Tables . . . . . **ix**

List of Figures . . . . . **xi**

1 Introduction **1**
1.1 Motivation 1
1.2 Previous Research 2
1.3 Contributions 6
1.4 Preliminary Work 6
1.5 Approach 9

2 Airframe and Solar Panel Design **11**
2.1 Introduction 11
2.2 System Layout 11
2.3 Photovoltaic Cell Theory 13
2.4 Determination of Power and Size Design Constraints 15
2.5 Drag Analysis 19
2.6 Design Method 21
2.7 Wing and Tail Design 26

3 Solar Tracker Design **33**
3.1 Introduction 33
3.2 Algorithm Design 33
3.3 Circuit Design 35
3.4 Interface Design 37

4 Final Design and Construction of the UAV **39**
4.1 Introduction 39
4.2 UAV Final Design 39
4.3 Tracking Versus Non-tracking UAV Design Comparison 42
4.4 Material Selection 43
4.5 Airframe Construction 44

5 Results 51
5.1 Introduction 51
5.2 Ground Testing of the Solar Panel 51
5.3 Battery Powered Flight Test 56
5.4 Solar Powered Flight Test 58
5.5 Analysis of Results 59
5.6 Global Applications 61

6 Conclusions 67
6.1 Summary 67
6.2 Conclusions 68

Bibliography 71

Appendix A. Tracker Controller Code 73

List of Tables

2.1 Typical motor and propeller data for NanSun obtained from MotoCalc v8.0 25

4.1 Some prevalent dimensions for NanSun 40

4.2 Some pertinent calculations relating to NanSun's power requirements 40

4.3 Makes and models of components used onboard NanSun 40

4.4 Weight breakdown of NanSun's members and components 41

5.1 Battery powered flight test results 58

List of Figures

1.1 NASA-funded Gossamer Penguin by AeroVironment 5

1.2 NASA-funded Pathfinder by AeroVironment 5

1.3 NASA-funded Centurion by AeroVironment 5

1.4 NASA-funded Helios by AeroVironment 5

1.5 AC Propulsion's SoLong UAV 6

1.6 Design space as a function of wing loading, power available, power required, and time of day with PV cells statically attached to the top surface of the wing 7

1.7 Design space as a function of wing loading, power available, power required, and time of day with PV cells on a solar tracking system 8

2.1 Layout of electronic hardware used onboard NanSun, and ground support hardware used for measuring Solar Irradiance 12

2.2 The assembled NanSun 13

2.3 Sample I-V curves and maximum power points for a PV array at different solar irradiance levels for Shell Solar Type IV Powermax Cells . . . 15

2.4 Sample I-V curves of a PV array at different cell temperatures for Shell Solar Type IV Powermax Cells 15

2.5 Flowchart of the optimizing iterative process for minimizing NanSun's P_{er} 25

2.6 2-dimensional Data for the Epplar 64 Airfoil 28

2.7 Types of dihedral layouts 29

2.8 Planform view of NanSun's wing 30

3.1 Basic control loop for NanSun's solar tracker controller 34

3.2 Photo Sensor mounted on the solar panel 36

3.3 Layout of the tracker controller photo sensor 36

3.4 Solar tracker system components 37

3.5 The UAV laying on its side 38

4.1 NanSun's assembled airframe, pictured with the solar tracking mode turned off and the horizontal panel mode turned on 42

4.2 The tail-fuselage junction and the trailing edge of the solar panel 45

4.3 NanSun's wing-setting piece on the fuselage 46

4.4 Structural panel for the array of PV cells 47

4.5 Array of PV cells 48

4.6 NanSun's wing assembly 49

4.7 NanSun's fuselage assembly 49

5.1 MPP voltage and current measurements from NanSun's solar panel 53

5.2 Power from NanSun's solar panel and from the MPPT output 53

5.3 MPPT efficiency 53

5.4 Portable radiometer and amplifier circuit 55

5.5 Amplified voltage signal of the radiometer 55

5.6 Power curve of the radiometer that correlates to the curve of power available from NanSun's solar panel 56

5.7 NanSun and the mock solar panel pictured prior to launch 57

5.8 NanSun flying during the solar powered flight test 59

5.9 Power gained by NanSun from solar tracking, and additional power required due to excess drag from the solar tracking system 61

5.10 Energy advantage of NanSun's solar tracking system as a function of the Earth's latitude angle, based on the energy available from NanSun's 6.06% efficient PV cells 63

5.11 Energy advantage of NanSun's solar tracking system as a function of the Earth's latitude angle, based on the energy available from 12.5% efficient PV cells 65

Chapter 1

Introduction

1.1 Motivation

The scope of electric powered unmanned aerial vehicle (UAV) missions is primarily constrained by the relatively low flight endurance that is characteristic of electric powered UAVs. The purpose in utilizing solar energy to power UAVs is to increase UAV endurance capabilities and ultimately achieve indefinite sustained flight. Traditional solar powered UAVs are designed to statically fix the photovoltaic (PV) cells on the top surface of the wing, keeping the cells virtually parallel to the earth's horizontal plane during normal flight. This puts significant restrictions on both where and what time of year a solar powered UAV is able to capture enough energy from the sun for the PV cells to be advantageous.

In order for solar powered UAVs to fly for any significant amount of time the UAV's geographical location on the earth must be a place where the angle between the sun's normal vector and the normal vector of the UAV's PV cells is small enough to provide the cells with adequate solar energy to power the UAV. Due to the fact that the PV cells are located on the lifting surfaces of traditional solar powered UAVs, the normal vector of the solar cells is nearly always co-linear with the normal vector of the earth's surface. This creates angles relative to the sun's normal vector that are not conducive to maximizing solar energy capture. Long flight endurance times of traditional solar

powered UAVs are also largely dependent on an environment where there is consistent rising air during the day, which requires advanced skill on the part of the pilot to find rising air and avoid downward rushing air. Due to these constraints there have been few solar powered UAVs that have successfully flown at all.

These constraints make any location that is significantly far away from the earth's equator a very poor environment for solar powered aircraft, especially in the winter when the sun's altitude angle is very low. Even at locations near the earth's equator, where the time of year is insignificant, the sun is nearly normal to the lifting surfaces of the UAV for only a few hours during the day.

Designing the PV cells to track the sun so that they are always perpendicular to the sun's incident rays, as this project has accomplished, is a viable method of broadening the geographical and seasonal constraint boundaries inherent with traditional solar powered UAV designs. No evidence or documentation of any such UAV with an onboard solar tracker has been found.

1.2 Previous Research

The first recorded solar flight was achieved by Astro Flight's Sunrise I in 1974. It was powered from PV cells mounted on the top surface of its wings, capable of a maximum of 450 W. It weighed 27.5 lb, and had a 32 ft wingspan. Sunrise I was damaged in a sand storm in 1975 [1].

In 1980, AeroVironment flew the solar powered Gossamer Penguin above Rogers Dry Lakebed at Edwards, California. This aircraft was manned, weighed 68 lb without the pilot, used 600 W of power from solar cells, had a wingspan of 71 ft, and made

numerous flights. Its solar panels were fixed at an angle to achieve high solar energy capture, as shown in Figure 1.1 [1].

AeroVironment was funded in 1981 to work on a classified solar powered UAV project for the U.S. government. They built HALSOL (High-Altitude Solar Energy), a UAV that was mothballed for about a decade. HALSOL later evolved into the solar UAV entitled Pathfinder, shown in Figure 1.2. Pathfinder could produce a maximum of 8,000 W from solar cells, weighed 486 lbs, and had a wingspan of 98 ft. In the mid 1990's, NASA's Environmental Research Aircraft and Sensor Technology (ERAST) program became interested in solar aircraft and Pathfinder became a part of NASA's ERAST program. On Sept. 11, 1995, Pathfinder set an altitude record for solar aircraft by climbing to 50,500 ft. The National Aeronautic Association presented the NASA-industry team with an award for one of the "10 Most Memorable Record Flights" in 1995. Pathfinder set the world altitude record for both propeller driven aircraft and solar powered aircraft in 1997 with an altitude of 71,530 ft. Pathfinder was later modified by an increase of wingspan to 121 feet and a replacement of the old PV cells with newer, more efficient cells. This increased the maximum power potential by another 4,500 W. This version, called Pathfinder Plus, flew to an altitude of 80,000 ft. in 1998 [2].

NASA continued to fund AeroVironment, who created Centurion in 1998 (Fig. 1.3). Centurion had a wingspan of 206 ft, weighed 1,300 lbs, and was powered with a PV array capable of capturing a maximum of 31 kW of solar power [3].

The latest of the larger NASA funded AeroVironment solar planes was Helios (Fig. 1.4). Helios set an impressive altitude record of 96,500 ft in the summer of 2001. It had a wingspan of 247 ft, weighed over 2,000 lbs, and was powered by a PV array

capable of capturing 42 kW of solar power [3]. One hour into a planned 20-hour test flight, Helios crashed into the Pacific Ocean and was destroyed in June 2003 [4].

The smallest solar powered aircraft that is known to have successfully flown is the PicoSol radio controlled airplane by Dr. Sieghard Dienlen. This small aircraft weighed 1.24 N and had a wingspan of .99 m [3].

An article by AC Propulsion entitled "AC Propulsion's Solar Electric Powered SoLong UAV" [5] discusses some details of the 4-year-long development of their solar powered UAV shown in Figure 1.5. In July of 2004, at the same site in California that the Gossomer Penguin was flown 30 years earlier, the solar powered SoLong flew for 48 continuous hours. SoLong was the first solar powered UAV of its size and class to successfully fly through the night and fully recharge its batteries during the day from the sun's power while remaining airborne. This feat was only accomplished in a desert with consistent thermals in the day, a time of year and location where high solar flux across the surface of the solar cells can be achieved, and by a team of skilled pilots taking turns in the "cockpit" from their ground station. SoLong had a nominal solar power capability of 225 W, a wingspan of 4 meters, a weight of 12.6 kg, and used a Maximum Power Point Tracker (MPPT) developed by AC propulsion that weighed 100 grams.

Fig. 1.1 NASA-funded Gossamer Penguin by AeroVironment

Fig. 1.2 NASA-funded Pathfinder by AeroVironment

Fig. 1.3 NASA-funded Centurion by AeroVironment

Fig. 1.4 NASA-funded Helios by AeroVironment

Fig. 1.5 AC Propulsion's SoLong UAV

1.3 Contributions

This work has developed a detailed parametric design for a solar powered UAV. The UAV is capable of tracking the sun. The UAV's solar panel can rotate about a single axis to track the sun's altitude angle, or the sun's angle up from the horizon. The sun's azimuth angle, or the angle along the horizon, is tracked by the UAV's flight path. A solar tracking prototype UAV has been developed from this design, and its power advantage over traditional UAVs with fixed solar cells has been shown. This thesis also relates equations and hardware selection methods used to minimize the theoretical power required for steady level flight at an optimal design velocity.

1.4 Preliminary Work

A project feasibility analysis was performed to determine how much solar power could be obtained in one day when PV cells align themselves normal to the sun's incident rays verses how much solar power is obtained with the common practice of fixing PV cells on the top surface of the wing, or in the horizontal plane. Based on the sun's

altitude angles in Provo, Utah for the duration of a clear June 21 day [6], design volumes were generated for both a tracking and a horizontally fixed solar panel under the assumption that each case has the same PV cell surface-area to planform-area ratio. These design volumes, illustrated in Figures 1.6 and 1.7, are constrained by the power available from the sun per weight for each case (represented by the upper surface) and the power required from the sun per weight for flight (represented by the lower surface, which is mostly hidden by the upper surface) as a function of wing loading and time of day. The intersection of the upper surface and the lower surface is depicted by the thick black curve in this figure.

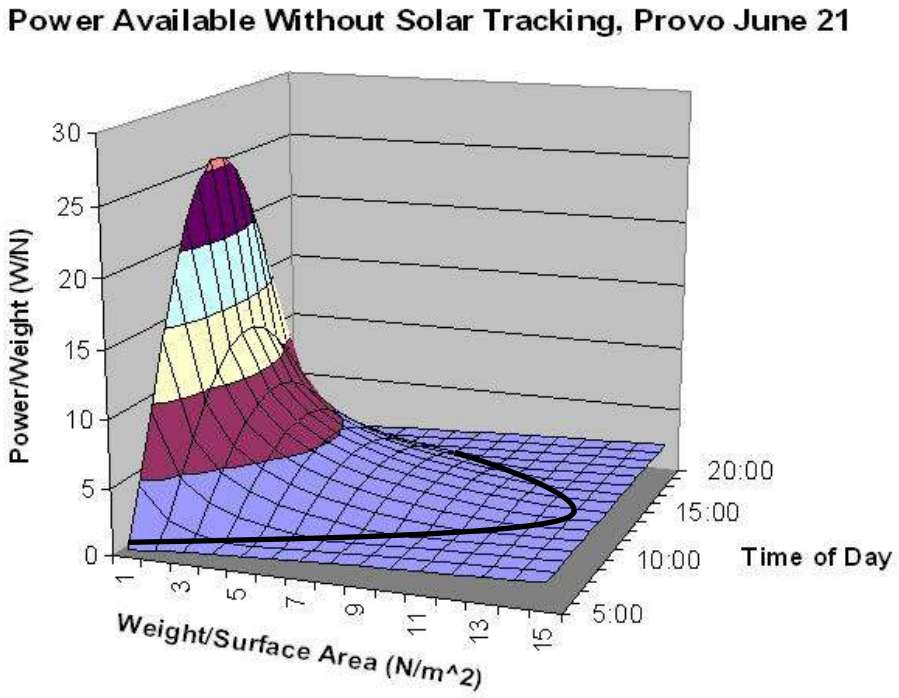

Fig. 1.6 Design space as a function of wing loading, power available, power required, and time of day with PV cells statically attached to the top surface of the wing

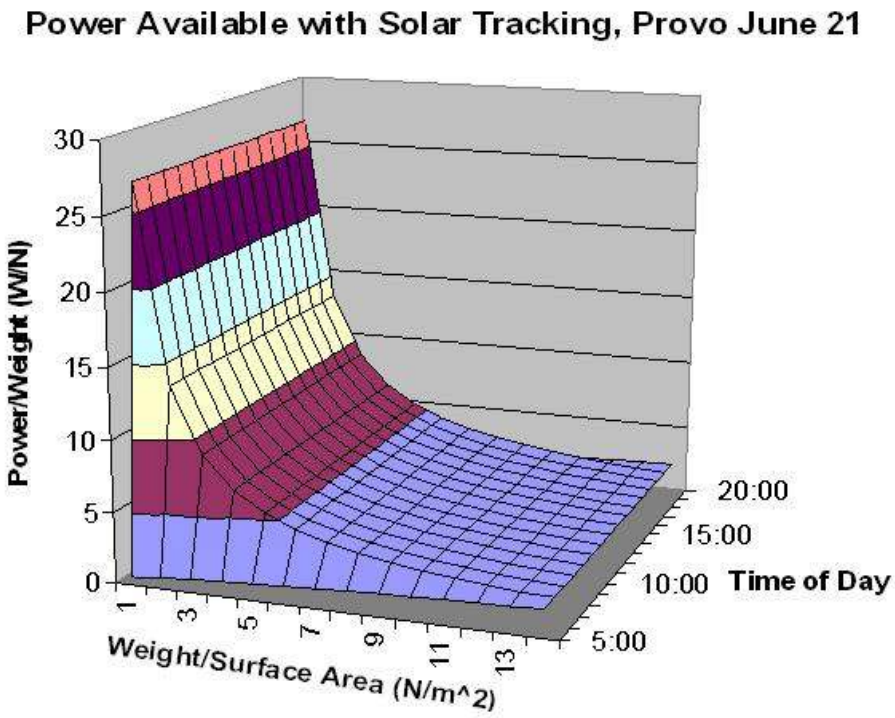

Fig. 1.7 Design space as a function of wing loading, power available, power required, and time of day with PV cells on a solar tracking system

From these figures it can be seen that in the case with solar tracking, a UAV has a larger window of time during the day when it can theoretically fly strictly from solar power. Compared to the non-tracking plane, the solar tracking plane also has greater excess available power at any hour while the sun is up. The accumulation of this excess power can be stored in a battery for flight after sundown, or when the UAV needs bursts of power.

This analysis shows that for any given wing loading, a UAV with the solar tracking system is capable of capturing 59% more energy for the whole day of June 21 than the same UAV with its PV cells fixed in the horizontal plane. This preliminary feasibility analysis did not take into account the extra power consumption associated with the components of the solar tracking system and their additional drag. Even with these

power loss factors, which were assumed to be significantly less than the 59% gross energy gain, an overall net energy capture increase is strongly suggested by this analysis. The drag analysis is discussed in Chapter 2. Even though the total energy available in a winter day is less than it is in a summer day, the difference in the percentage of energy gained from employing a solar tracker would be even more drastic in the winter. The theoretical amount of energy available with the solar tracking PV cells is only dependent on how long the sun is up, whereas the amount of power available to the horizontal PV cells is dependent on both the sun's altitude and azimuth angles in addition to how long the sun is up.

1.5 Approach

An efficient airframe capable of housing the autonomous onboard solar tracker was designed around the minimum number of PV cells necessary for solar flight. This design was done parametrically to allow for an efficient optimization process. The flight components were selected so that they would be operating near their peak efficiencies at the UAV's optimal velocity for minimizing the power required for steady level flight. The power benefits of the onboard solar tracker were then verified with solar panel ground tests, and with flight tests of a UAV that was fabricated according to the parameters found from the parametric design. This prototype UAV has been given the name NanSun.

Chapter 2

Airframe and Solar Panel Design

2.1 Introduction

Designing an efficient airframe is a key component for achieving successful solar powered flight. PV cell arrays typically do not allow for high power applications unless a large number of cells are connected together. The design program that this work presents was constructed parametrically in a series of spreadsheets. The parametric design facilitated a fast and accurate optimization of interdependent parameters to minimize the power required for steady level flight.

This chapter discusses the theory and methods used for determining the system requirements for NanSun. The system's component and power requirements are established, and the method used for modeling drag is discussed. The optimization process for minimizing NanSun's required power for flight is presented, as is the design of NanSun's lifting and stabilizing surfaces.

2.2 System Layout

The functional requirements of the system led to the inclusion of many components in the UAV. The onboard system of electronic components and their interactions are shown in Figure 2.1. The bottom portion of this figure also shows the ground support equipment used during flight and the system used to measure solar

irradiance. This measuring system is described in Chapter 5. The bold italicized components in this figure are not commercially available. They were custom designed and fabricated specifically for this UAV. The methods used for selecting the other components, which are commercially available, are described in the following sections of this chapter.

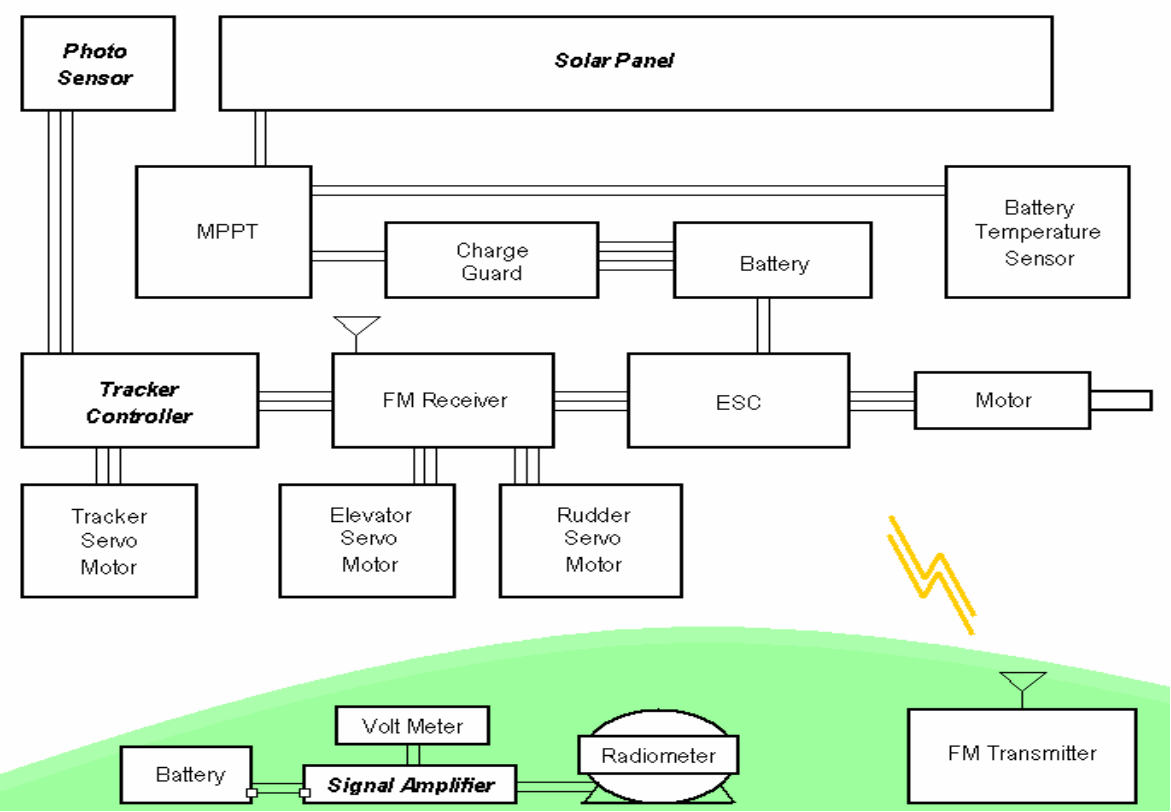

Fig. 2.1 Layout of electronic hardware used onboard NanSun, and ground support hardware used for measuring Solar Irradiance.

The general aerodynamic design process of NanSun followed that of conventional tailed aircraft, with the exception of the added tracking solar panel. It was necessary for the axis of rotation for the tracking solar panel to be parallel to the free stream velocity vector. This was to ensure that the solar panel maintained a zero degree angle of attack

with respect to the free stream regardless of its position as it tracks the sun. This led to the need of a long fuselage, and a conventional tailed aircraft design is conducive to this constraint.

It was decided that the solar panel should be positioned above the fuselage and wings, as shown in Figure 2.2, for a couple of reasons. First, this would keep any shadows from the wings or fuselage from diminishing the effectiveness of the solar panel. Second, this configuration protects the fragile solar panel from damage during landings, regardless of its angle relative to the ground at the time of landing.

Fig. 2.2 The assembled NanSun. The tracker controller rotates the solar panel about the carbon rod that is attached to the tail's vertical stabilizer and the front tracker support panel.

2.3 Photovoltaic Cell Theory

To understand the most prevalent power constraints imposed on a solar powered aircraft, it is first necessary to understand some fundamental principals of PV cell operation. The maximum available power from a PV cell or a PV array of cells is

directly proportional to the solar irradiance it receives. Also, maintaining the load resistance on the array at an optimal value is imperative in order to achieve maximum available power from the array. There is a point on a PV array's current-voltage curve (*I-V* curve) where power, the product of current and voltage, is at a maximum. Some *I-V* curves for an array made up of the same PV cells that are used in NanSun are shown in Figure 2.3. The circles on each curve in this figure represent the maximum power point at each irradiance level. These curves illustrate the relationship between current and voltage for a PV array.

For any solar powered application where the load on the PV array varies with time, a Maximum Power Point Tracker (MPPT) must be used in order for the PV cells to operate at any reasonable level of efficiency. A MPPT keeps an optimal load on an array of PV cells by adjusting the load impedance to match the internal impedance of the PV array. It keeps this optimal load resistance on the PV array regardless of the varying power demands of the system powered by the array. This optimal load keeps the PV array operating at the point on its *I-V* curve where power output is at a maximum.

The temperature of the PV cells also affects their efficiency, as shown in Figure 2.4. The power loss due to cell temperature is of sufficient significance to consider cooling methods in solar powered UAV applications. The solar panel on NanSun was convection cooled by the free stream air, as there was no encapsulation or covering over the cells on the solar panel.

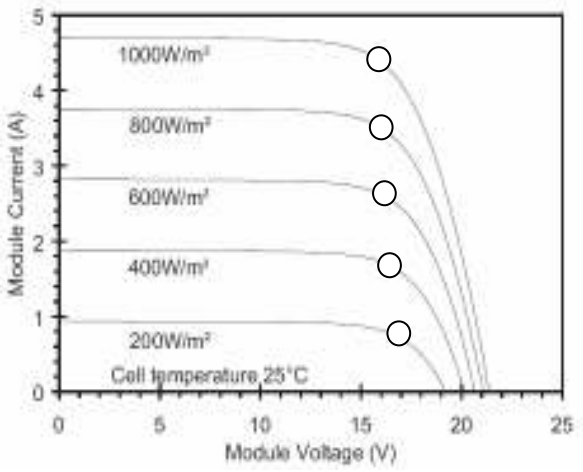

Fig 2.3 Sample I-V curves and maximum power points for a PV array at different solar irradiance levels for Shell Solar Type IV Powermax Cells

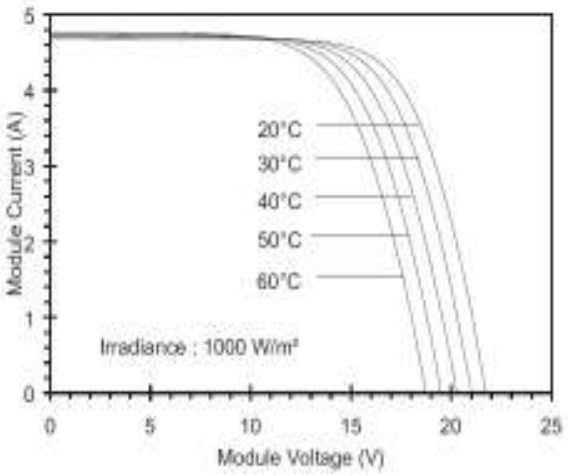

Fig 2.4 Sample I-V curves of a PV array at different cell temperatures for Shell Solar Type IV Powermax Cells.

2.4 Determination of Power and Size Design Constraints

Before the detailed parametric design of NanSun could be constructed, a rough size estimate and power requirement of the UAV needed to be obtained. Due to limited resources and the need to easily transport the UAV, small size was deemed to be important. The minimum possible size of NanSun was primarily constrained by the minimum allowable number of PV cells that could supply a high enough voltage for the MPPT to function efficiently.

The MPPT used in NanSun has a recommended operable input voltage range between 15 and 30 V, and two output levels of either 14.1 or 28.2 V. It was designed to charge lead acid batteries. The output voltage at either level can be adjusted to some degree with a trim potentiometer on the MPPT printed circuit board. The output voltage was adjusted to be 12.6 V to coincide with the charging requirements of a lithium polymer battery pack consisting of three cells connected in series. A lithium polymer

battery pack was chosen because of its extremely high energy density compared to other battery types and its high discharge capabilities.

The maximum voltage of the lithium polymer batteries used in NanSun, as with most lithium polymer packs, is 4.2 V per cell. The maximum charging voltage of these cells is 4.25 V per cell, but a cell will charge at a lower supply voltage so long as the supply voltage is greater than the voltage on the cell. Charging a lithium polymer battery pack at a voltage greater than 4.25 V per cell will cause permanent damage to the cells and creates a potential fire hazard. Thus the ideal charging voltage range desired for charging a 3-cell lithium polymer battery pack is between 12.6 V and 12.75 V, where 12.75 V is the maximum allowable value.

It was found through testing of the MPPT that there is a specific input voltage range that yields an output between 12.6 V and 12.75 V. This acceptable voltage range was determined experimentally. Solar power in this experiment was simulated with a laboratory DC power supply as the MPPT input. The PV cells used on NanSun were PowerMax Type IV cells from Shell Solar. According to the specifications provided by Shell Solar, the Maximum Power Point (MPP) current and voltage of each cell at Standard Test Conditions (STC) is 4.25 A and .458 V respectively. Shell's STC values are defined to be a solar irradiance level of 1,000 W/m^2 and a temperature of 25 C.

The MPP current value was simulated with the DC power supply by holding current constant at the PV cell's MPP current value, 4.25 Amps. The DC power supply voltage was varied manually to simulate a differing number of PV cells connected in series. A discharged 3-cell lithium polymer battery pack was used as the load and was attached to the MPPT output leads. It was found that MPPT input voltages that were less

than 14.1 V yielded an output voltage less than 12.6 V, and a MPPT input voltage greater than 19.2 V yielded an output voltage greater than 12.75V. This defined the acceptable input voltage range for the MPPT. Any MPPT input voltage outside of this acceptable range yields an output voltage that is either too high for safe charging conditions, or too low to charge the battery pack to its full capacity.

The acceptable MPPT input voltage range was used to determine how many PV cells should be connected in series to power the UAV. Based on Shell's STC data, 42 cells operating at their MPP voltage of 0.458 V per cell yield a voltage of 19.23 V, which is almost exactly equal to the upper limit of the acceptable MPPT input voltage. Assuming that the PV cells will always be operating at or below their maximum efficiency voltage, a solar panel with 42 cells connected in series should not produce a MPPT input voltage that exceeds the upper limit of 19.2 V.

The power available from a solar panel connected to a MPPT is given by

$$P = n\eta_{MPPT} I_{MPP} V_{MPP} \cos\phi, \tag{2.1}$$

where P is power in Watts, n is the number of PV cells connected in series, η_{MPPT} is the efficiency of the MPPT, I_{MPP} is the maximum power point current, V_{MPP} is the maximum point voltage, and ϕ is the angle of the sun's incident rays with respect to the normal of the solar panel face. The maximum power possible ($P_{\max}$) from the solar panel occurs when ϕ is zero. According to Shell's specifications, and taking into account a 5% power loss from the MPPT's specified operating efficiency, a PV array with 42 cells connected to the MPPT should yield a maximum power of 77.7 W.

These power attributes led to the selection of an optimal 3-cell lithium polymer battery pack. The primary purpose of the battery in this system was to act as a buffer between the solar panel and the UAV's power consuming components. When the UAV required more power than could be provided by the solar panel, such as while it was climbing, it drew extra power from the battery. When the solar panel provided more power than was needed by the plane, the excess power was stored in the battery. Lithium polymer batteries cannot be safely charged at a rate higher than one times their capacitance. Since I_{MPP} of the solar panel was 4.25 Amps, the smallest and therefore lightest battery that could safely be used in NanSun is a 4.25 Amp-hour pack. The closest commercially available pack found was a 4.4 Amp-hour pack, so it was selected for use in NanSun.

A charge guard circuit designed specifically for the lithium polymer batteries used in NanSun was connected between the MPPT output and the battery charge input. This acted as a failsafe against voltage spikes and overcharging. This charge protector cuts all current to the battery if the charge voltage exceeds 4.25 V per cell.

A 3 by 14 PV cell matrix was chosen as the configuration of the 42 cell solar array. This gave the solar panel a length of 1.825 m and a width of .395 m including the 5 mm clearance between each cell for wiring and fixturing purposes. Configuring the solar panel to have less than 3 rows would force the fuselage to be excessively long and difficult to transport.

The required size of the solar panel provided a guideline for the general sizing of the rest of the airframe. The maximum available power of 77.7 W from the solar panel was the primary constraint used for selecting the other electrical components and

establishing a weight budget so that NanSun would be able to fly purely from solar power.

2.5 Drag Analysis

A thorough drag analysis is necessary in order to obtain an accurate drag prediction. An accurate drag prediction is important when designing solar powered aircraft, which are marginally powered by nature.

The overall coefficient of drag (C_D) for an aircraft is the sum of the induced drag coefficient (C_{Di}) and the parasite drag coefficient (C_{Do}) as shown in Eq. (2.2).

$$C_D = C_{Di} + C_{Do} \tag{2.2}$$

Although some C_{Di} is produced at the tail under dynamic flight conditions, the wing is the only member assumed to produce any C_{Di} on NanSun. For the vast majority of NanSun's time in the air, the stabilizers have near zero angle of attack and thus negligible induced drag. The relationship that was used for finding C_{Di} on NanSun is

$$C_{Di} = \frac{C_L{}^2}{e\pi AR}. \tag{2.3}$$

C_L is the coefficient of lift. The Oswald efficiency factor (*e*) was found according to the equation

$$e = 1.78\left(1 - 0.045 AR^{0.68}\right) - 0.64 . \tag{2.4}$$

This relationship for e is a function of aspect ratio (AR), and assumes a straight wing [7]. It was therefore a conservative estimate of e for NanSun's double tapered wing. The design of NanSun's wing is discussed further in Section 2.7.

The coefficient of parasite drag for a subsonic aircraft is given by

$$C_{Do} = \sum_i C_{M\,i} + \sum_j C_{INT\,j} + C_{FORM} + C_P . \tag{2.5}$$

The first summation is the sum of each individual member's parasite drag coefficient, and the second summation is the sum of interference drag coefficients where members come together. The C_M value for each individual member was found with the equation

$$C_M = \frac{s_m}{S} C_{fe} . \tag{2.6}$$

S is the planform area of the wing, s_m is the wetted surface area of the airframe member, and C_{fe} is the effective friction coefficient, given by

$$C_{fe} = (1.5)\frac{1.328}{\sqrt{\mathrm{Re}}} \tag{2.7}$$

for laminar flow or

$$C_{fe} = (1.5)\frac{0.42}{\ln^2(0.056\,\mathrm{Re})} \tag{2.8}$$

for turbulent flow [8]. Laminar flow was assumed for the wings, and turbulent flow was assumed for the solar panel because of its length. Turbulent flow was also assumed for the fuselage and the stabilizers because they are located directly behind the propeller.

The coefficient of form drag (C_{FORM}) was assumed to be zero in the design of NanSun, as care was taken to streamline the trailing edges of all members to a point. The protuberance drag coefficient (C_P) is difficult to predict accurately, especially in a solar powered aircraft where there are many very small protuberances on the solar array. In the design of NanSun, C_P was accounted for by adding an extra 20% onto the overall drag coefficient, C_D .

2.6 Design Method

All calculations performed in the parametric design of NanSun assumed steady level flight. That is the flight mode that the UAV was designed to take on for the vast majority of its time in the air. Ideally, the only exceptions would be at takeoff, landing, and during turns. This model assumes a wide enough turn radius for the steady level flight assumption to always hold true. At the heart of the design are two equations of flight. These equations are

$$W = L = \frac{1}{2}\rho V^2 C_L S \tag{2.9}$$

and

$$T_r = D = \frac{1}{2}\rho V^2 C_D S. \tag{2.10}$$

For steady level flight, the UAV weight (W) equals lift (L), and the thrust required (T_r) equals the UAV's drag. The air density is ρ and V is the free stream velocity, or velocity of the UAV. The required planform area of the wing can be found by solving Eq. (2.9) for S such that

$$S = \frac{2W}{\rho V^2 C_L}. \tag{2.11}$$

The power required (P_r) for steady level flight is the product of the drag and the free stream velocity, so the electrical power required by the motor (P_{er}) for steady level flight can be calculated from the equation

$$P_{er} = \frac{VT_r}{\eta_{mp}}. \tag{2.12}$$

The efficiency of the motor-propeller combination (η_{mp}) was obtained from MotoCalc v8.0. This efficiency factor also included the motor's loss of efficiency from its gearbox. Designing an efficient airframe for NanSun required finding an optimum design velocity that minimizes P_{er}. When C_L was optimized with V to minimize P_{er}, the optimal C_L for

NanSun was dangerously close to $C_{L\max}$, where stalling would occur. The value for NanSun's lift coefficient was chosen to be significantly less than $C_{L\max}$. The optimization process that was used to minimize P_{er}, depicted in Figure 2.5, is described below.

First a weight for the aircraft had to be assumed. Initially, the weights of many of the components and structural members of NanSun had to be estimated. To ensure P_{er} remained less than $P_{\max}$ of the solar panel, conservative estimates for the members with unknown weights were initially used. These estimates ended up being very close to the actual weights. As pieces of the UAV were fabricated and weighed, the weight in the design was updated.

Next a motor-propeller combination was chosen in order to obtain η_{mp}. For any motor-propeller combination for which MotoCalc has data, MotoCalc is able to generate a table of performance characteristics for different flight velocities. Table 2.1 shows some of these performance characteristics at several different airspeeds for the motor-propeller combination that was chosen for use in NanSun. Possible motor-propeller combinations for NanSun were found by trying many different motor-propeller combinations in MotoCalc until a group of combinations was found that had a thrust output greater than T_r and required less power than P_{er} at the optimum design velocity. The models of motors and propellers in this group of possible combinations were also required to be in stock and available from at least one vendor so that they could be purchased for use in NanSun. From this group of candidates, the motor-propeller

combination with the highest η_{mp} at the optimum design velocity was selected for use in NanSun.

The next step in the process was varying V in Eq. (2.12) to make P_{er} a minimum. This was done with the solver function in Microsoft Excel, which was set to perform 1,000 iterations per function call. The values of the parameters that are dependent on velocity changed parametrically in the design spreadsheets when the new optimal V was found. This optimization was subject to the constraint that L must equal W. As the weight and design velocity of NanSun changed, so did the wing area according to Eq. (2.11). In order to keep the wing span from going to infinity and the chord from going to zero during the optimization, AR was constrained to be less than or equal to eight. Constructing a lightweight aircraft with an AR greater than eight would be difficult to manufacture, to transport, and also would also pose structural problems on hard landings.

Once the optimum V was found, the currently selected motor-propeller combination was again compared to other combinations. This comparison was done in case the final optimum V varied enough from its original value, before the iterative process, to make a new motor-propeller combination better than the current selection. In that case, the η_{mp} value from the new motor-propeller combination was substituted into Eq. (2.12) and the iterative process was repeated. This process was also repeated each time the design weight was updated and approached the actual weight. Every time an update was made and the optimization was performed, it was verified that P_{er} remained less than $P_{\max}$.

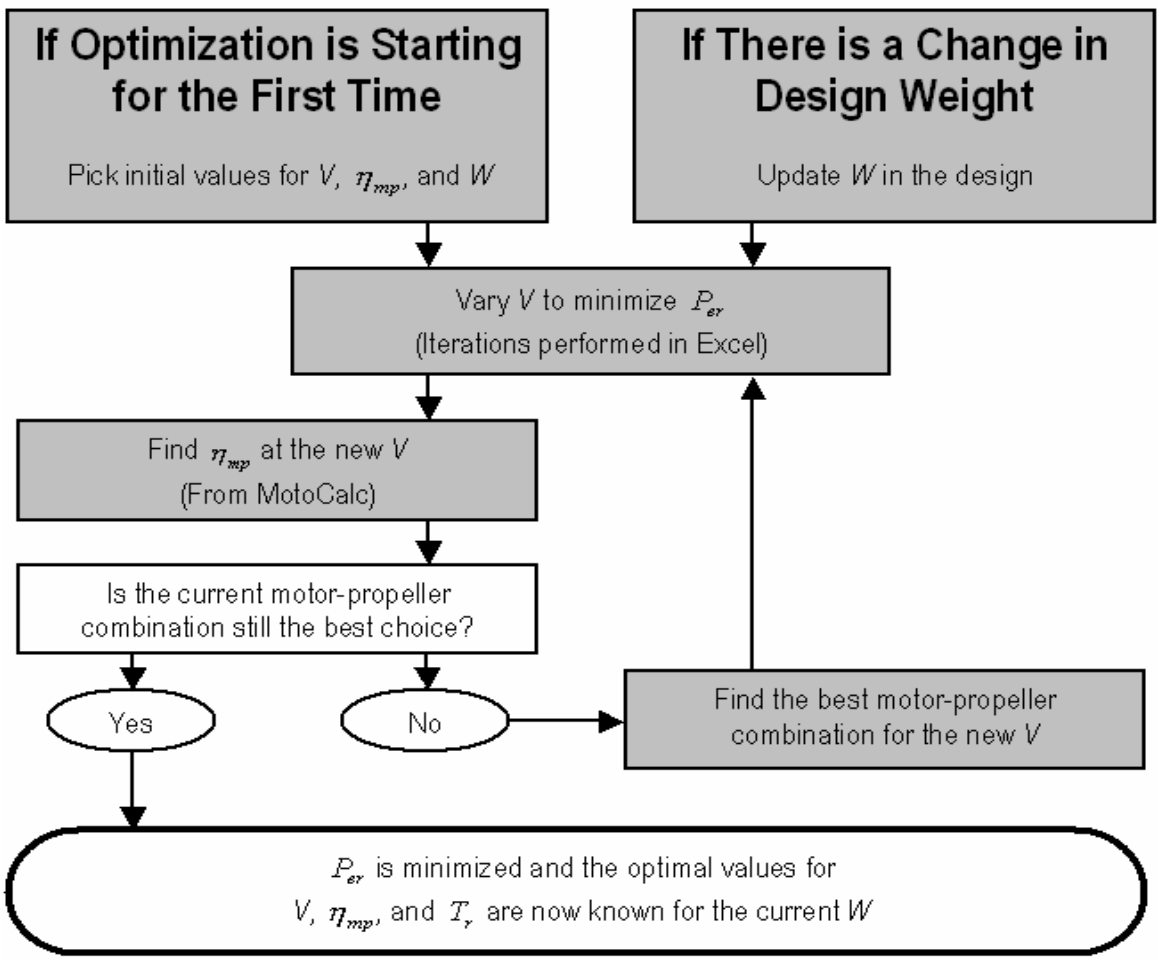

Figure 2.5 Flowchart of the optimizing iterative process for minimizing NanSun's P_{er}

Table 2.1 Typical motor and propeller data for NanSun obtained from MotoCalc v8.0. The data pertaining to NanSun's optimum V are shaded.

Air Speed (mph)	Power Required (W)	Shaft Efficiency (%)	Prop Efficiency (%)	Total Efficiency η_{mp} (%)	Thrust (oz)	Motor RPM	Prop RPM
⋮	⋮	⋮	⋮	⋮	⋮	⋮	⋮
18	55.6	75.0	66.3	49.8	13.2	9279	2109
19	53.8	75.2	67.8	51.0	12.4	9333	2121
20	51.6	75.4	69.0	52.1	11.5	9397	2136
21	49.2	75.6	70.1	53.0	10.6	9470	2152
22	46.4	75.8	70.9	53.8	9.6	9552	2171
⋮	⋮	⋮	⋮	⋮	⋮	⋮	⋮

The final motor-propeller combination consisted of a high performance geared brushless motor and a large folding propeller. A folding propeller was selected to protect it from damage during landings, and also to reduce drag during un-powered flight. A geared motor-propeller combination was deemed to be best for this low power application because of its low current draw, and because of its ability to drive a large propeller. A direct drive system would require a smaller propeller with a lower pitch to keep the motor from operating inefficiently in an overloaded condition. The overall efficiency gained by using a larger propeller with a higher pitch was significantly greater than the extra 5% efficiency loss from the motor's gearbox. The η_{mp} value for the combination chosen for use in NanSun was 52.1% at the optimum V. The best direct drive motor-propeller combination found using MotoCalc that still met NanSun's power requirements had an efficiency of 30.3%. Due to the system's relatively low current draw, the battery efficiency was assumed to be 100%.

2.7 Wing and Tail Design

The Epplar 64 airfoil was chosen for use in the wing. One reason is that it provides enough thickness to make a structurally sound wing. Another reason is that it has favorable lift and drag characteristics for Reynolds numbers near that of NanSun, about 220,000, as can be seen on the left portion of Figure 2.6 [9]. After C_L was chosen, the angle of attack (α) corresponding to that C_L for the airfoil had to be found. A 3-dimensional finite wing experiences a reduction in lift and an increase in drag due to air leakage at the wingtips from the lower surface to the upper surface. Therefore, the slope of the line that relates C_L and α is less than the slope of the line in the right side of

Figure 2.6 that relates c_l and α, where c_l is the 2-dimensional coefficient of lift. The slope of the line that relates C_L and α ($C_{L\alpha}$) is found by

$$C_{L\alpha} = f \frac{c_{l\alpha}}{\left(1 + \frac{c_{l\alpha}}{\pi AR}\right)}. \tag{2.13}$$

In this relationship $c_{l\alpha}$ is the slope of the line $c_l(\alpha)$ and f is the reduction factor. The reduction factor is usually between 0.96 and 1.0 for AR greater than 3, and was chosen to be 0.97 for NanSun [8]. The α value that corresponds to C_L for NanSun was then found according to the equation

$$\alpha = \frac{C_L}{C_{L\alpha}} + \alpha_o. \tag{2.14}$$

The angle of zero lift (α_o) for this airfoil is –4.5°, as seen at the point that $c_l(\alpha)$ intersects the x-axis in Figure 2.7.

For a rudder steered UAV such as NanSun, dihedral is necessary in order to initiate a banked turn [10]. An advantage to keeping the wings of the UAV free of PV cells is that dihedral can easily be incorporated into the wing, and the dihedral will not compromise the effectiveness of the PC cells. Dihedral also provides roll stability, and inherently returns a banked aircraft to level flight. The more dihedral built into a wing, the greater the roll stability and the turn response will be. However, too much dihedral

results in poor performance in crosswinds, and poor damping for Dutch-roll instability [11].

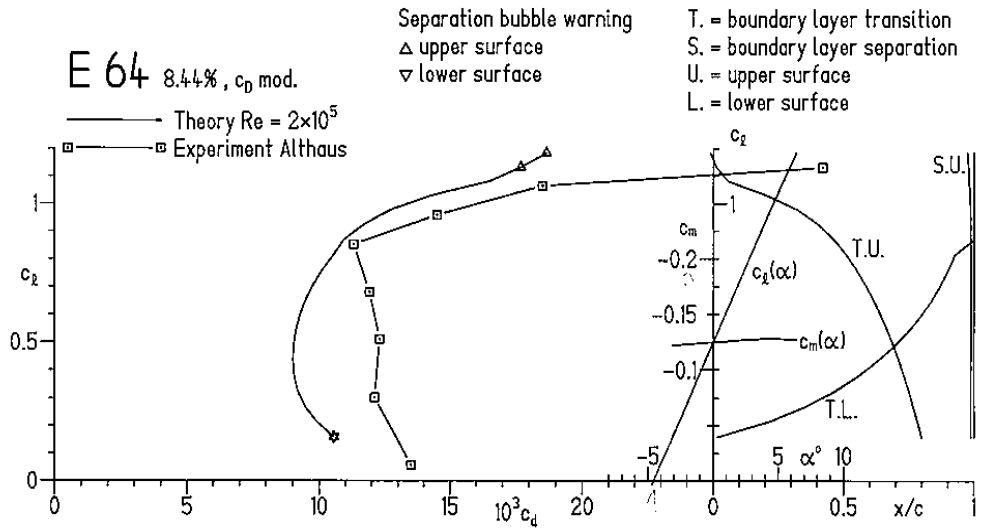

Fig. 2.6 2-dimensional Data for the Epplar 64 Airfoil

The most efficient type of dihedral is elliptical in form, but arc dihedral is difficult to manufacture. NanSun's wings were constructed with four discreet panels at varying angles. This layout, called polyhedral, was used to approximate the ideal elliptically shaped arc dihedral. Various types of dihedral layouts, including polyhedral, are portrayed in Figure 2.7. NanSun's wing was designed to provide an effective dihedral angle (*EDA*) equal to 11.5^o for added stability.

A lightweight airframe is necessary for marginally powered aircraft, such as NanSun. The wings constituted a large enough portion of the UAV to merit a structural analysis. This was done to ensure that no more composite material would be added to the wings than was necessary. Superfluous composite material in a member as large as the

wings would result in a significant and unnecessary weight increase. A safety factor of 1 was deemed appropriate in this analysis because the model was very conservative. It assumed that all lift acts at the wingtips and all weight acts at the root. Keeping the wings free of PV cells proved to be advantageous from a structural standpoint as well. With no PV cells on them, wings are allowed to deflect under load without breaking the cells.

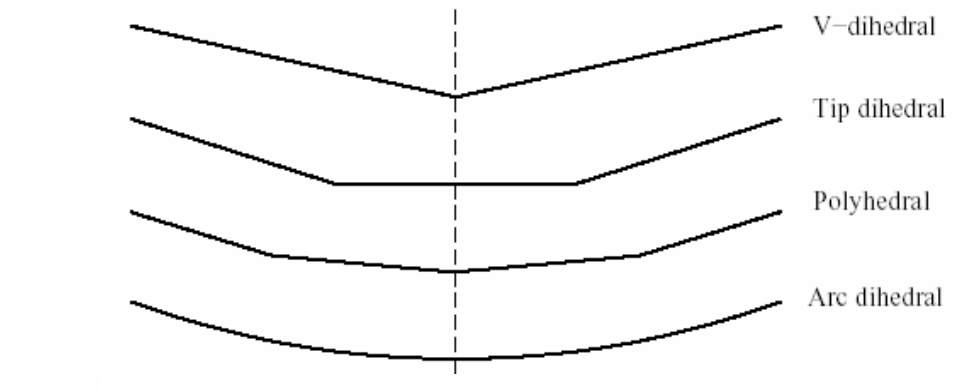

Fig. 2.7 Types of dihedral layouts, with the least efficient at the top and most efficient at the bottom.

An elliptical wing planform produces an ideal elliptical lift distribution. The double tapered wings that constitute NanSun's planform approximate an ellipse. A projection of NanSun's planform shows this double taper (Figure 2.8). The constraint on the minimum chord length at the wingtips requires the *Re* to stay at least 20% above the critical *Re* value for the Epplar 64 airfoil. This critical *Re* value of 100,000 is where the Epplar 64 airfoil begins to be susceptible to flow separation [9]. This failsafe against wingtip stalling was used instead of adding washout, as washout does not produce the

most efficient wing possible [10]. The fact that this UAV never needs to make tight turns also guards against inner wingtip stalling.

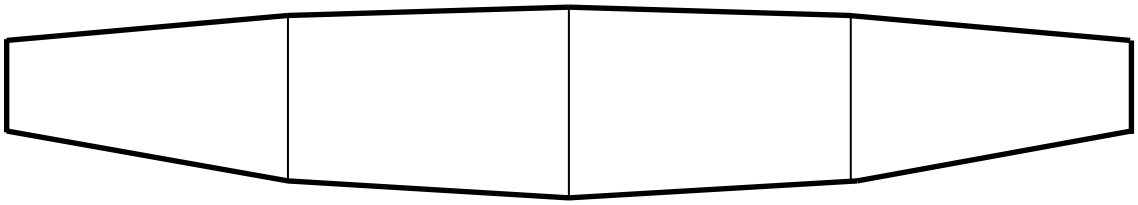

Fig. 2.8 Planform view of NanSun's wing with the leading edge at the top.

During the design portion of this project, there was some uncertainty as to how well NanSun would respond to control input while housing a large moving solar panel. For this purpose the tail volume ratio of both the horizontal and vertical stabilizers on NanSun was about double that of most commercially available radio controlled thermal gliders. A symmetrical airfoil was used for these stabilizers, and the thickness was determined according to the equation

$$t_{opt} = \frac{1.63c}{\mathrm{Re}^{1/4}}. \tag{2.15}$$

The optimal thickness to help minimize drag is t_{opt}, and c is the chord length of the stabilizer. This equation is recommended for surfaces with Reynolds numbers that are less than 10^6 [12]. As mentioned in Section 2.6, the tail was assumed to have virtually no angle of attack relative to the free stream. This gave a tail-setting angle of $-\alpha$ from the wing. This was the same setting angle as the other members that were inline with the free

stream under steady level flight conditions. These members were the motor, fuselage, solar panel, and tail.

Once the design and the optimization processes were established, the optimal flight parameters for minimizing NanSun's P_{er} could quickly be found. The design process described in this chapter provided a quick and accurate method for finding the necessary design parameters for the solar powered UAV, even after alterations in weight, size, or components were made.

Chapter 3

Solar Tracker Design

3.1 Introduction

The solar tracker system was comprised of a microcontroller based tracker controller board, a photo sensor, a servo, and a mechanical four-bar linkage that rotated the solar panel. Keeping both weight and power consumption low were important design specifications for this system. It was designed to autonomously find and track the altitude angle of the sun that maximized solar energy capture by the solar panel. Again, the UAV's flight path must be perpendicular to the sun's rays in order to capture maximum possible solar energy. This chapter presents the design of NanSun's solar tracking system. The tracker controller circuit design is discussed, as well as the control algorithm for the tracker.

3.2 Algorithm Design

The programming language used for this application was PicBasic Pro, which was developed exclusively for PIC microcontrollers. The architecture for the tracker controller program is depicted in the flowchart shown in Figure 3.1. The tracker controller code is included in Appendix A.

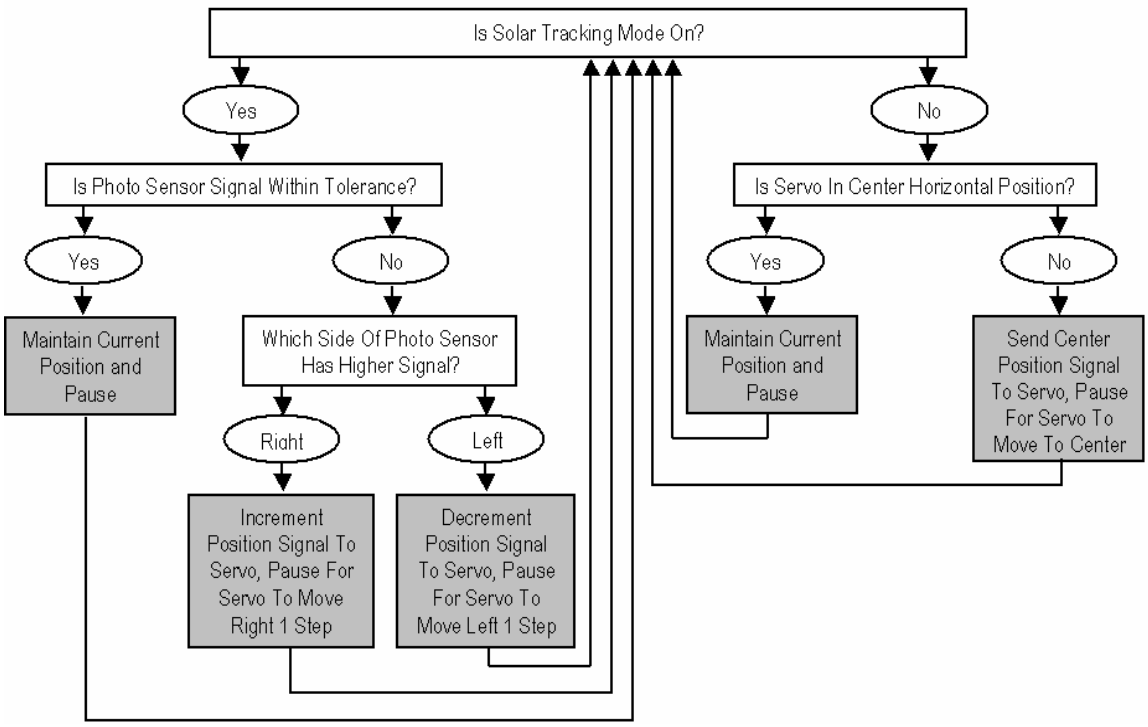

Fig. 3.1 Basic control loop for NanSun's solar tracker controller.

In addition to the tracker autonomously tracking the sun, it also needed the ability to move and hold the solar panel to be in its horizontal position. This override function was included to prevent adverse aerodynamic effects in the case of crosswinds blowing over the solar panel. It was also included for safer launches and landings in the case of crosswinds. In the unlikely event that the solar panel would situate itself such that the photo sensor was shaded from the sun, this panel centering function could return the sensor to sunlight to resume tracking. The pulse from the landing gear channel on the FM receiver was used as the input to the tracker controller. Thus the landing gear switch on the FM transmitter could toggle between two modes of operation: solar tracking panel mode and stationary horizontal panel mode.

Under normal flying conditions, the tracker system should not need to move the solar panel very frequently or very far once the panel reached its optimal angle relative to the sun. The tracker controller was programmed to only send new positioning signals to the servo if the signal from the photo sensor was outside a certain tolerance range. This saved energy consumption by preventing the servo from constantly jittering back and forth as it attempted to find the exact angle of maximum solar flux. Jittering servomotors are constantly operating in a nearly stalled condition, and therefore require significantly more power than servos operating normally.

3.3 Circuit Design

The PIC16F877A microcontroller was chosen for use in the tracker controller because of its memory capacity and the vast amount of documentation available on how to troubleshoot this particular model. The circuit board was designed to connect to NanSun's FM receiver for operating mode input and power.

The photo sensor was mounted onto the solar panel, as shown in Figure 3.2. It was designed to produce a voltage difference between its left and right side while not pointing directly at the sun. A pair of photocells was connected in parallel on each side of the sensor as shown in Figure 3.3. The resistance of a photocell is dependent on the intensity of the incident light on its face. The topmost two photocells in Figure 3.2 were positioned 45^{o} away from the normal of the solar panel face. The bottom two were facing 90^{o} away from the solar panel's normal so that one side of the sensor still received sunlight when the solar panel was facing away from the sun. This configuration ensured that when the resistances (and therefore voltages) of both sides of the sensor were equal, the solar panel was at the angle of maximum solar irradiance.

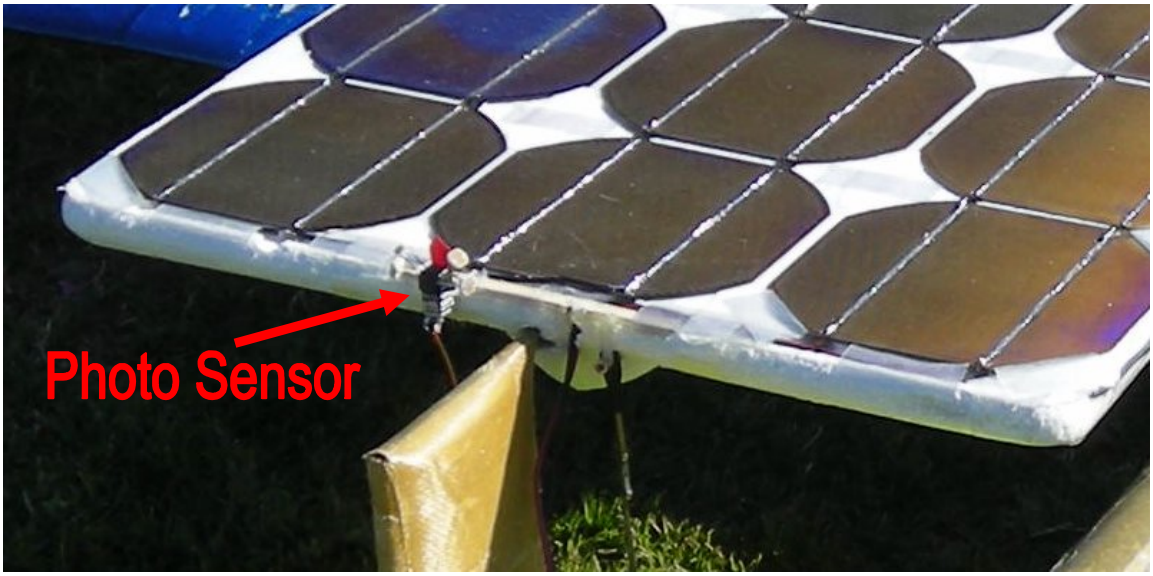

Fig. 3.2 Photo Sensor mounted on the solar panel.

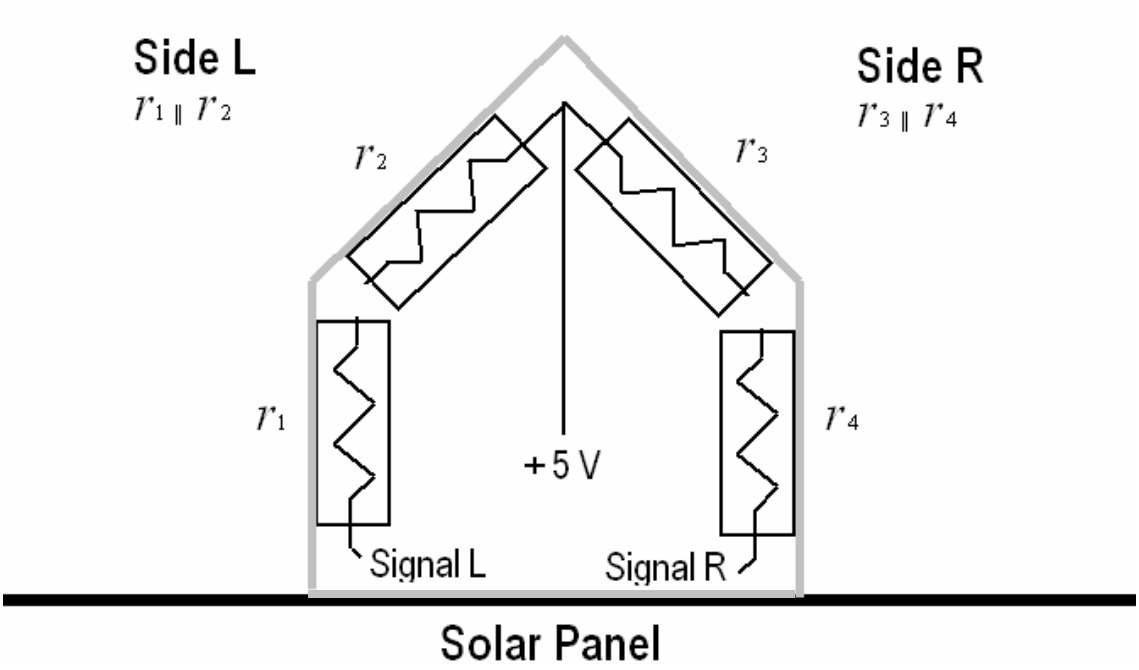

Fig. 3.3 Layout of the tracker controller photo sensor, consisting of four photocells. Note that r_1 is parallel to r_2 and r_3 is parallel to r_4.

Due to variance between photocells, some bias error existed between the two sides of the sensor. To overcome this problem, a trim potentiometer was connected

serially to the signal wire of the right side of the photo sensor. The trim potentiometer was mounted onto the tracker controller board. The photo sensor could thus be fine-tuned to make the solar panel face the sun exactly by adjusting the trim potentiometer. The photo sensor and tracker servo are shown plugged into the tracker controller board in Figure 3.4.

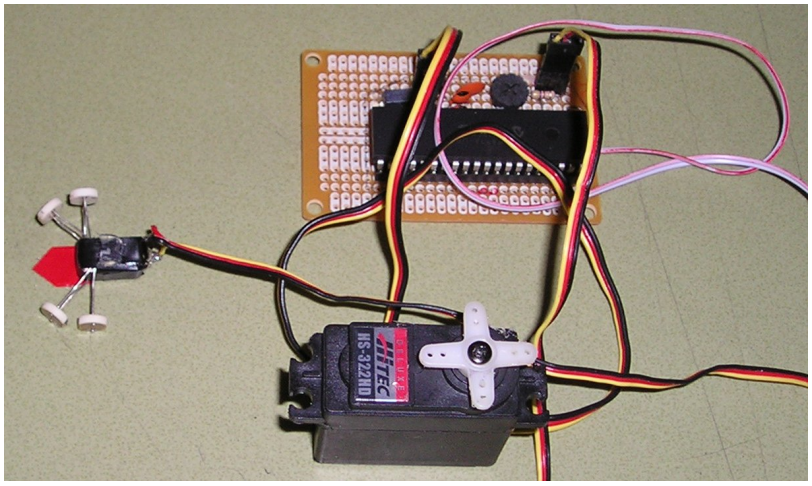

Fig. 3.4 Solar tracker system components: photo sensor, tracker controller board, and servo.

3.4 Interface Design

The solar panel's axis of rotation was placed as close to the center of gravity of the panel as was possible. This was done to minimize aerodynamic forces on the solar panel so that the tracker servomotor would not be overstressed. The model of servo chosen to control the solar panel, the Hitec HS-322HD, is commonly used for control surfaces on large radio controlled aircraft. It has a stall torque of 4.25 inch-pounds.

A four-bar linkage was used to interface the tracker controller servo with the solar panel. The links are highlighted in white in Figure 3.5. The servo's range of motion was

set to be 180^{o} by the tracker controller, or $\pm 90^{o}$. The linkage was designed to make the solar panel's range of motion 160^{o}, which gave the solar panel $\pm 80^{o}$ of rotational capability from its horizontal position. Were the solar panel allowed any more rotation, the wings would begin to shade its surface during level flight.

Fig. 3.5 The UAV laying on its side. The solar tracker four-bar linkage is highlighted in white. The servo body is housed in the fuselage, and the servo arm link is protruding out of the side of the fuselage.

On completion of the airframe design and solar tracker design, UAV construction could commence. The construction and final design of NanSun is discussed in the following chapter.

Chapter 4

Final Design and Construction of the UAV

4.1 Introduction

Predictive model validation cannot be accurate without a physical model that very closely represents the analytical model. Nor can much be learned from a poorly or sloppily constructed prototype. A great deal of detailed craftsmanship was invested into the construction of NanSun to ensure quality performance, and to ensure that the UAV matched what the analytical model was designed to predict. NanSun also had to be designed for efficient assembly and disassembly to accommodate transportation and storage needs. This had to be done without adding unnecessary weight and protuberances.

This chapter presents some of the key final design parameters for NanSun. The findings from a comparison between NanSun's design and a non-solar tracking version of NanSun are given in order to quantify the power penalty of onboard solar tracking. Reasoning for the materials that were selected is also discussed, as well as some of the fabrication processes that were undergone to create the physical model of NanSun.

4.2 UAV Final Design

Many parameters and variables were used in the design process of NanSun. The UAV's most defining dimensions and parameters are shown in Tables 4.1 and 4.2. The

purchased components selected for use onboard NanSun are listed in Table 4.3. A weight breakdown for each member of NanSun is listed in Table 4.4. The fully assembled NanSun is pictured in Figure 4.1.

Table 4.1 Some prevalent dimensions for NanSun

Key Geometry Calculations	
Wing	
Surface Area (m^2)	1.28
Wing Span (m)	3.2
Mean Chord (m)	0.4
Aspect Ratio	8
Dihedral of inner wing panel (degrees)	5
Dihedral of outer wing panel (degrees)	15
EDA (degrees)	11.495
Ave Taper Ratio (wing and tail)	0.660
Center of Gravity Location from LE (m)	0.096
α From Line of Thrust	3.640
Tail and Fuselage	
Span of Vertical Stabilizer (m)	0.684
Ave Chord of Vertical Stabilizer (m)	0.208
Span of Horizontal Stabilizer (m)	1.350
Ave Chord of Horizontal Stabilizer (m)	0.208
Fuselage Total Length (m)	2.870
Solar Panel	
Solar Panel Length (m)	1.825
Solar Panel Width (m)	0.395

Table 4.2 Some pertinent calculations relating to NanSun's power requirements

Key Power Calculations	
Velocity (m /s)	9.14
C_L	0.70
Total weight (*N*)	40.44
Total Drag (*N*)	3.12
L/D	12.98
Weight / Surface Area (N/m^2)	31.60
η_{mp}	52.03%
P_{er} (*W*)	54.74
P_r (*W*)	28.48
$P_{\max}$ of PV Array (*W*)	77.64
% Excess Power Predicted	**41.83%**

Table 4.3 Makes and models of components used onboard NanSun

Component	Make	Model
Motor	Hacker	B40 12L
Gearbox	Hacker	B 4:1
Propeller	Aeronaut	CAM Carbon 13x17
ESC	Hacker	Master 48-3 BEC
Receiver	Hitec	Electron 6
Control Servos	Hitec	HS-85MG
Tracker Servo	Hitec	HS-322HD
Battery	Hi-Po	PQ-4400SP-3S
Charge Guard	Poly-Quest	PQPCM3S
MPPT	Solar Converters Inc.	PT 12/24-5

Table 4.3 - Continued

PV cells	Shell Solar	Power Max Type IV
Microcontroller	PIC Micro	PIC16F877A
FM Transmitter	Hitec	Eclipse 7

Table 4.4 Weight breakdown of NanSun's members and components.

Component	Unit Weight (g)	Quantity	Weight Sub Total (g)	% of the Total UAV Weight
Structure			**2084**	**50.54%**
Wing	911	1	911	22.09%
Wing attachment	63	1	63	1.53%
Boom Fuselage	720	1	720	17.46%
Vertical stabilizer	90	1	90	2.18%
Horizontal stabilizer	160	1	160	3.88%
Push horns and rods	30	1	30	0.73%
Ultracote	110	1	110	2.67%
Electronics, propulsion			**636**	**15.42%**
Motor	131	1	131	3.18%
Gearbox	54	1	54	1.31%
Propeller	25	1	25	0.61%
ESC	39	1	39	0.95%
Receiver	18	1	18	0.44%
Servo	17	2	34	0.82%
Battery	297	1	297	7.20%
Charge Guard	18	1	18	0.44%
Wiring	20	1	20	0.48%
Solar Energy System			**1403.8**	**34.04%**
MPPT	121	1	121	2.93%
Tracker controller	30	1	30	0.73%
Tracker servo	45	1	45	1.09%
Tracker axis rod	50	1	50	1.21%
PV cell panel	511	1	511	12.39%
PV solder, tabs, wires	2	42	84	2.04%
PV cell	13.4	42	562.8	13.65%
Total Weight (g)			**4123.8**	

Fig. 4.1 NanSun's assembled airframe, pictured with the solar tracking mode turned off and the horizontal panel mode turned on

4.3 Tracking Versus Non-tracking UAV Design Comparison

The final detailed design of NanSun provided the means to more accurately predict the difference in power gain between a UAV with a solar panel that tracks the sun and a non-tracking UAV. This comparison was performed using the parametric design spreadsheets that were created for NanSun.

The electrical power required for NanSun to sustain steady level flight was calculated. Using the same design, the power required for a non-tracking version of NanSun was calculated. The drag contribution of the tracking solar panel and the front tracker support spar was removed from the design for the non-tracking version calculation. The power consumption of the servo that rotates the solar panel was also

removed from the design. If the PV cells were mounted on the wings, the fuselage could be shortened to half its length. The drag contribution of the extra length of fuselage was also removed from the design. Cutting the length of the moment arm to the tail in half would normally require an increase in tail volume ratio. Due to the fact that NanSun was designed with an oversized tail volume ratio, no change in tail size or drag was assumed for the tail. The total increase in power required to fly with the tracking panel was 16.8%. This comparison also assumed no net change in weight between the two planes. That is, the weight lost from removing the tracking panel was assumed to equal the additional weight required to stiffen the wings sufficiently to safely support the PV cells. Chapter 1 presented a potential gross power gain of 59% from tracking the sun on June 21 in Provo, Utah. Assuming the tracking solar panel is achieving maximum solar irradiance 75% of the time, the gross power gain becomes 44.3%. This conservative estimate assumes that during the other 25% of the time, the plane is tacking toward or away from the sun or the solar panel is in the process of positioning itself to face the sun after a turn. Despite the 16.8% power penalty for housing the solar tracker, there is still a net power gain of 27.6% on the day of the year that solar tracking is least advantageous.

4.4 Material Selection

The primary considerations for selecting material for use on NanSun were weight and strength. In the interest of saving weight, almost every member on NanSun was a composite covered foam core part. The members that were covered with composite materials had a polystyrene foam core, while members that needed more flexibility were made from expanded polypropylene (EPP) foam. Polystyrene foam is more fragile and

less impact resistant than EPP foam, and therefore was used in composite reinforced members. EPP foam was used in members that needed the ability to elastically deform.

All members were covered in a lightweight iron-on membrane called Ultracote, except for the fuselage, which was covered in lightweight packaging tape. These coverings provided a smooth surface finish over the entirety of the plane.

4.5 Airframe Construction

Every member of the airframe was custom made specifically for NanSun. All blunt corners were sanded smooth and all trailing edges were sanded to fine points on every member of NanSun, including on the rudder and elevator. This was done to minimize form drag as much as possible. All of the electronic components in NanSun were housed within one of the UAV's aerodynamic members to minimize protuberance drag. Surfaces were blended where members were joined together to decrease interference drag. These blends were made with styrene foam and were covered with composite material, or Ultracote, or both. The rudder and elevator were made of balsa wood and were covered in Ultracote. Examples of how members were shaped to decrease interference drag and form drag are shown in Figure 4.2

The foam cores for the wings, tail stabilizers, and tracker support spar were cut with a CNC hotwire foam cutter. A Kevlar composite was molded over the leading edges of the stabilizers, and over the entire tracker support spar. A fiberglass composite was molded over the leading edge of the wings to give them structural support as discussed in Section 2.7.

Fig. 4.2 The tail-fuselage junction (left) and the trailing edge of the solar panel (right) display how the members of NanSun were blended and shaped to minimize form drag and interference drag.

The main fuselage member was comprised of extruded polystyrene foam surrounded by carbon fiber and Kevlar composite material. The diameter of the fuselage was made to match that of the UAV's nosecone. The foam core of the fuselage was hollow in the middle so the elevator and rudder servo control wires could be run to the tail internally. At the front of the fuselage, a member was added to act as housing for many of NanSun's electronic components, and to act as a skid during landing. This member was made of expanded polypropylene (EPP) foam covered in Ultracote. It was shaped to fit smoothly with the main fuselage member. The EPP foam member provided a protective cushion for the electronics that it housed as a guard against hard landings.

A wing-setting piece (Figure 4.3) was made to set the wings at the correct angle of attack relative to the other surfaces. This EPP foam piece was cut with the CNC hotwire foam cutter to match the shape of the wings at their root and to match the cylindrical shape of the fuselage to which it attaches. The wing and the wing-setting piece attached to the UAV with metal clips and rubber bands. Latex rubber was coated on the surface of the wing-setting piece that mated with the wings, as well as the surface

that mated with the fuselage. The latex rubber was added to help prevent the wing-setting piece from slipping on the fuselage, and to help prevent the wing from slipping on the wing-setting piece once they were attached to the plane. This system made it easy to move the wings forward and backward on the fuselage, which ensured that they were positioned correctly relative to the center of gravity of the plane.

Fig. 4.3 NanSun's wing-setting piece on the fuselage

The base component of the tracking panel for the PV cells was a polystyrene foam plank. A hollow carbon rod with the same length as the plank was set in the middle of the plank. This rod, which was fixed to the plank, acted as the outer bearing for the panel to rotate about. The inner bearing rod was a carbon rod that was thinner and longer than the outer bearing rod, and could spin freely inside the outer bearing rod. On the underside of the plank, directly over the panel's axis of rotation, a beam was attached to

stiffen the panel by giving it a larger moment of inertia. This beam was made of expanded polystyrene foam that was cut by the CNC hotwire cutter. The assembly was then covered with a thin fiberglass composite. This panel is shown in Figure 4.4. The 42 solar cells that make up the PV array were all soldered in series as shown in Figure 4.5

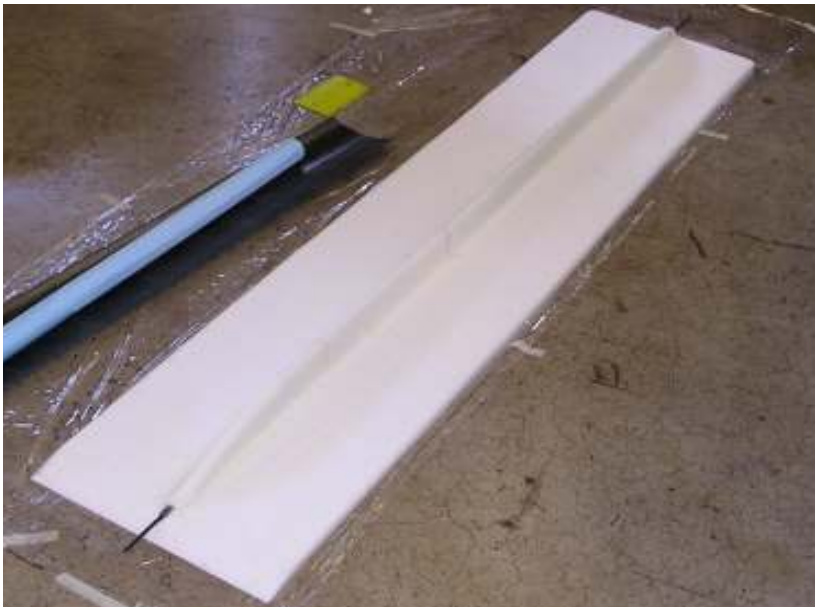

Fig. 4.4 Structural panel for the array of PV cells

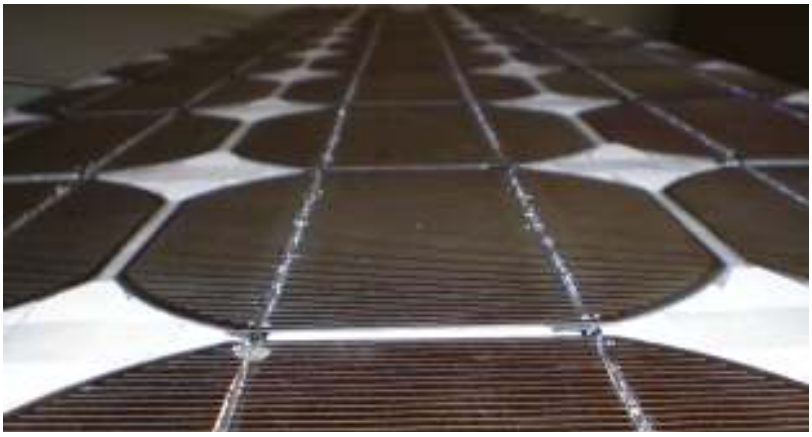

Fig. 4.5 Array of PV cells

With a length of 2.8 meters and a wingspan greater than 3 meters, the UAV needed to be built for assembly and disassembly so it could be transported and stored easily. The wings were designed to pull apart into two pieces, and press fit together via a pair of pegs and sockets as shown in Figure 4.6. The solar panel was designed to attach and detach from the plane in one piece. The fuselage was designed to attach and detach near the middle, as shown in Figure 4.7. These two parts press fit together. The plugs for the servo control wires, which run all the way through the center of the fuselage from the receiver in the front to the servos in the tail, are also shown.

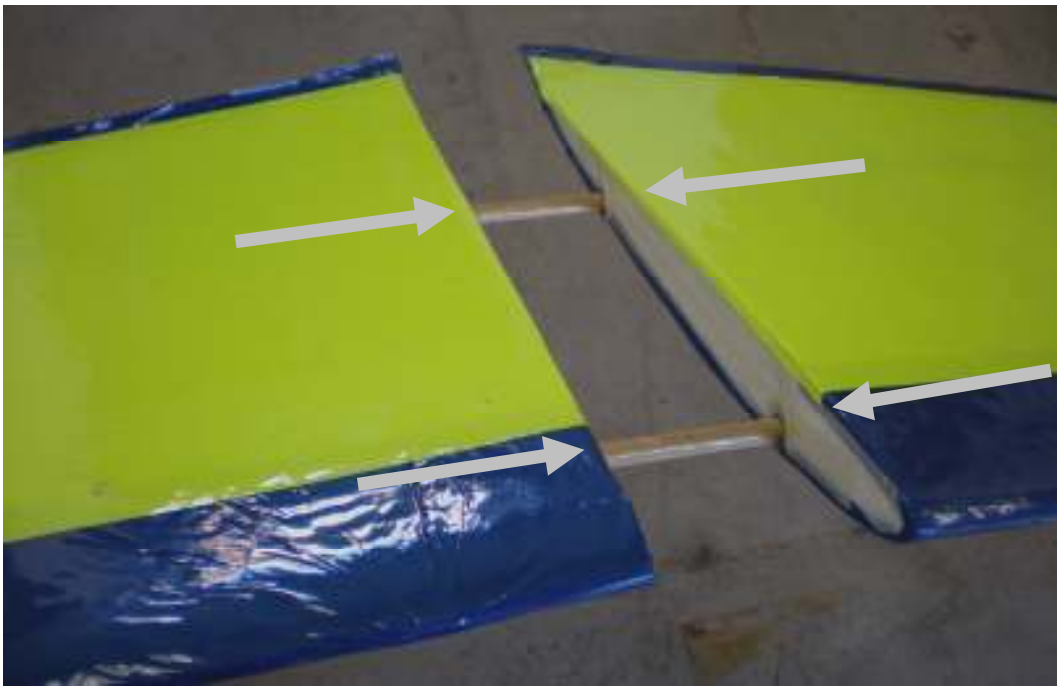

Fig. 4.6 NanSun's wing assembly

Once every member of NanSun was constructed, complete assembly and disassembly of the system was performed to verify rigidity of the airframe and overall functionality of the UAV. Testing of the system is described in the following chapter.

Fig. 4.7 NanSun's fuselage assembly.

Chapter 5

Results

5.1 Introduction

A series of tests were performed with NanSun in order to gain an understanding of how well the system worked in actual application and to validate the UAV's analytical model. Operation of the solar panel and tracking system was tested on the ground. A battery powered flight test and a solar powered flight test were also performed. This chapter presents the data that was found, and presents what can be learned from these tests. The test data was used to predict how NanSun would perform at various latitude locations around the world.

5.2 Ground Testing of the Solar Panel

These tests were conducted to measure the power available from NanSun's solar panel, and to verify that the solar tracker functioned as it was designed to function. NanSun was taken into full sunlight, and was positioned so that the solar panel's axis of rotation was perpendicular to the sun's rays. This simulated the ideal flight path of the UAV that would track the sun's azimuth angle. The tracker controller was then engaged, and the solar panel positioned itself to face the sun. NanSun was then yawed 180^{o} to simulate a turn in the air, and the solar panel positioned itself accordingly to face the sun. The solar tracking mode was then remotely turned off from the FM transmitter, and the

solar panel positioned itself to be horizontal. Other variations of this solar tracker test were performed to verify that the solar tracking system was reliable.

The solar tracking linkage was then disengaged, and the solar panel was rotated to various angles relative to the sun's incident rays. At each angle, voltage and current were measured at both the solar panel's output, and at the MPPT's output (Figure 5.1). This data was all taken within a timeframe of 15 minutes, so uniform atmospheric conditions were assumed for each reading. From this data, power available from the solar panel and the MPPT efficiency were plotted versus angle of incident light from the normal of the solar panel (ϕ). These plots are shown in Figures 5.2 and 5.3. As discussed in Section 2.4, the acceptable MPPT output voltage range was between 12.6 V and 12.75 V. The range for ϕ that yielded voltages within this acceptable MPPT output range was $\pm 7^{o}$. The accuracy of the solar tracking system was $\pm 1.2^{o}$, so the $\pm 7^{o}$ tolerance was easily kept. The maximum voltage measured was 12.66 V.

Voltage and current measurements were also taken at the ϕ value for which the solar panel was horizontal. This ϕ represents the angle of incident light that would be seen by the solar array of a UAV with PV cells that are fixed to its wings. The data points relating to this ϕ value are signified by the vertical dashed-line in each of the figures below. These tests were all performed on a clear sunny day between 1:50pm and 2:05pm on November 10, 2006 in Provo, Utah.

The maximum power measured from the MPPT output was 37.7 Watts. The maximum power predicted for the system was 77.7 Watts based on the specifications for the solar cells that were used. This was a 51.5% power deficit compared to the predicted value, and was not adequate for NanSun to fly purely from solar energy. The specified

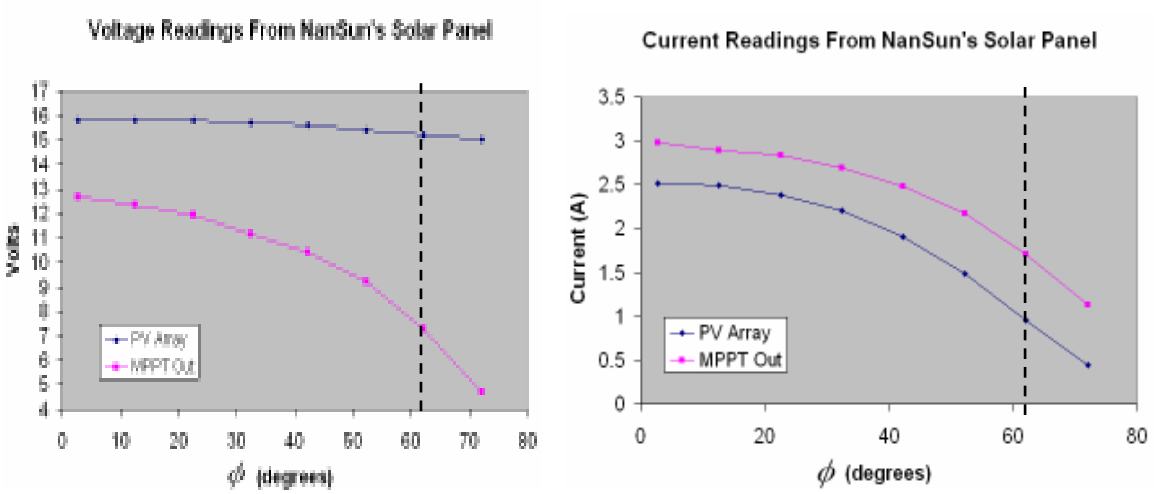

Fig. 5.1 MPP voltage and current measurements from NanSun's solar panel. The vertical dashed-line represents the incident light angle with respect to the solar panel's normal when the solar panel is horizontal. Voltage accuracy was ± 0.01 V and current accuracy was ± 0.01 A, assuming a 95% confidence interval.

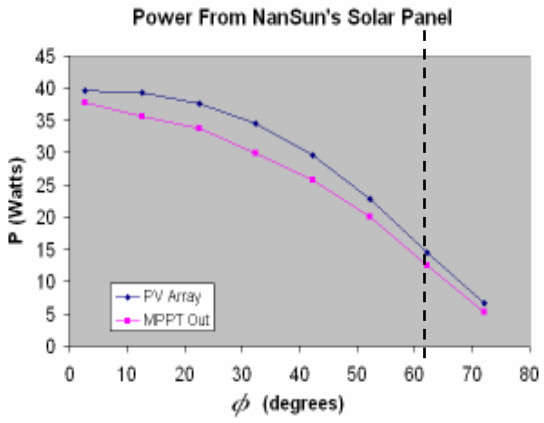

Fig. 5.2 Power from NanSun's solar panel and from the MPPT output. Accuracy is ± 0.79 W.

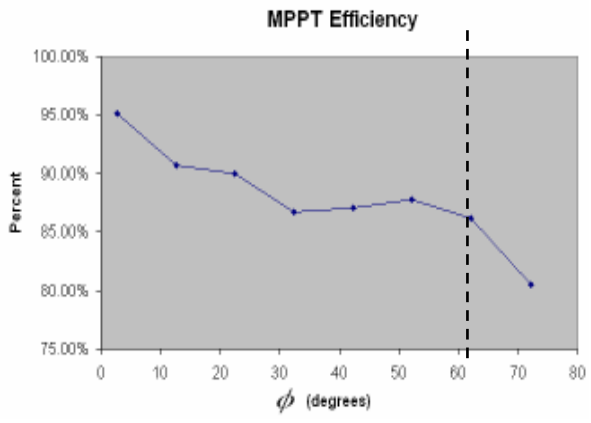

Fig. 5.3 MPPT efficiency. Accuracy is ± 4.2%.

PV cell efficiency for these cells is 12.5%, and the actual measured efficiency was 6.06%. This deficit may have stemmed from a couple of sources. One possibility for this power deficit is that imperfections may have been imposed on the solar panel due to hand

fabrication. The solar cells were designed for assembly into solar panels using precision robotic machinery. Another possibility is that the solar cells themselves may have been flawed. The total energy that the tracking solar panel could capture for the entire day of November 11, 2006 in Provo, Utah was found to be 42% greater than the energy that the solar panel could capture if it were fixed horizontally.

The MPPT maintained a minimum of 15 volts at its input while it was operating, as seen on the left side of Figure 5.1, and this caused its efficiency to suffer at high ϕ values. The MPPT efficiency was therefore dependent on the solar panel's angle of incident light, as seen in Figure 5.3. Although the data points in this figure are somewhat sporadic, they suggest that MPPT efficiency increases as ϕ decreases. The maximum MPPT efficiency occurred when ϕ was near zero, and was found to be 95.1%. This is very close to the MPPT's specified efficiency of 95%. This suggests that the MPPT was not a cause for the power deficit between the actual and predicted maximum power available values.

A radiometer was used to measure solar irradiance so that the solar energy available from the solar panel could be recorded from the ground while NanSun was in the air. The radiometer was tested at the same time that the solar panel was tested. A correlation between incident light on the radiometer and on the solar panel was found. The output of the radiometer was a low voltage signal, and was amplified with an operational amplifier circuit to ensure accurate data recording with a voltmeter. This ground support hardware for measuring solar irradiance is shown in Figure 5.4. The response of the radiometer's amplified signal is shown in Figure 5.5. This amplified signal was related to NanSun's solar panel according to the equation

$$P_i = K \frac{V_R}{G} A_P C_{fit} . \tag{5.1}$$

P_i is the power available for capture by the solar panel. K is a constant that relates the voltage signal of the radiometer to solar irradiance, and is equal to 82035 $\frac{W}{m^2} \Big/ V$ according to the radiometer's specifications. The amplified voltage signal from the radiometer is V_R, the gain of the operational amplifier circuit is G, and A_P is the area of the solar panel. C_{fit} is a scaling constant that makes the maximum P_i value equal to $P_{\max}$ of the solar panel. This correlation appears to be good for normal incident light angles less than 50^o, as can be seen in Figure 5.6.

Fig. 5.4 Portable radiometer and amplifier circuit

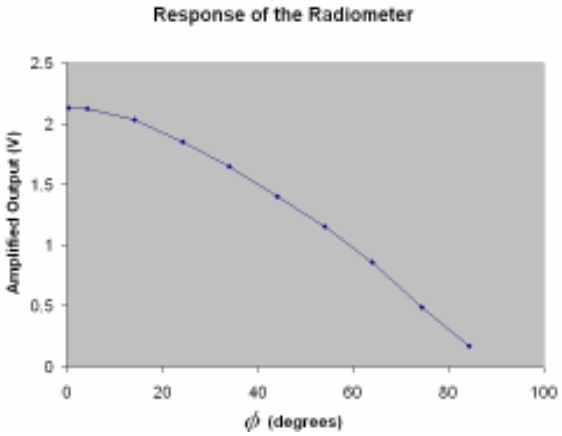

Fig. 5.5 Amplified voltage signal of the radiometer. Accuracy is ± 0.02 V.

After the solar data had been recorded, functionality of the solar charging system was tested. One of NanSun's discharged battery packs was connected to the charge

guard's output leads. Solar tracking mode was turned on, and the system successfully charged the battery pack.

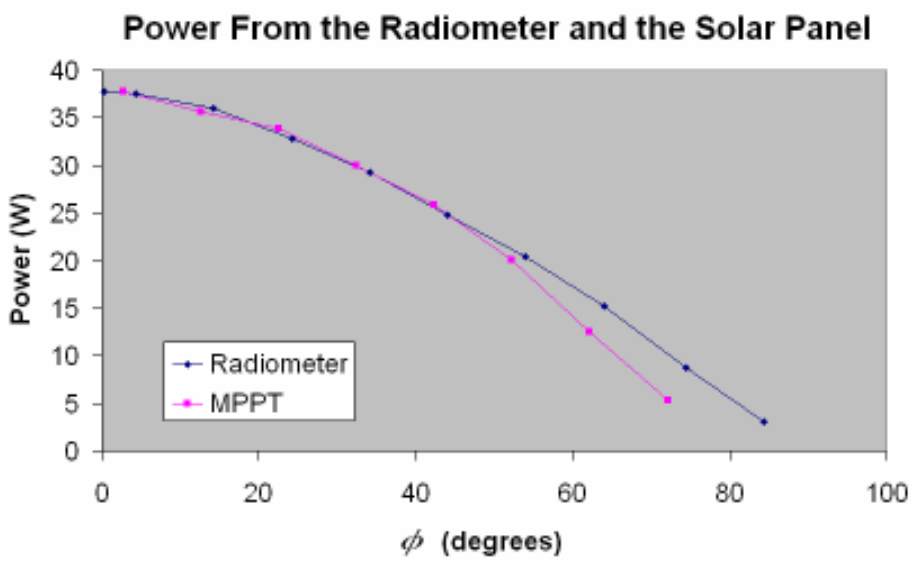

Fig. 5.6 Power curve of the radiometer that correlates to the curve of power available from NanSun's solar panel. Accuracy of the MPPT power and the radiometer power are ± 1.57 W and ± 2.70 W for ϕ values less than 50 ^{o}.

5.3 Battery Powered Flight Test

This flight test was powered only by NanSun's onboard battery pack. It was performed to validate the analytical model of NanSun's airframe, and to verify the UAV's ability to easily be piloted for steady, level, and controlled flight. A mock solar panel was used in place of NanSun's real solar panel. The mock panel was primarily made up of a cardboard plank that was re-enforced with fiberglass spars, and was the same size and weight as the real solar panel. The mock panel was fixed to be horizontal to avoid the complications of incorporating the tracker system onto the mock panel. The mock panel mounted on NanSun is pictured in Figure 5.7.

Fig. 5.7 NanSun and the mock solar panel pictured prior to launch

On December 9th, 2006 NanSun flew for 7 minutes and 55 seconds in Spanish Fork, Utah. The energy consumed by the UAV on this test flight was found by recording how much charge the battery accepted when it was recharged. NanSun's analytical model predicted how much energy the UAV would consume from a flight of this duration. The analytical model predicted that NanSun would require 41% less power than it actually did require. This error described how accurately the analytical model predicted the actual P_{er} of the system. This error could be the result of many factors. One source of error could stem from the fact that the analytical design assumed constant steady level flight, but the flight test included many dynamic turns and a climb from ground level. Another source of this error could be attributed to battery inefficiency. Another source of error could be from an actual flight velocity that differed slightly from the optimal design velocity. The results of this battery powered flight test are shown in Table 5.1.

Table 5.1 Battery powered flight test results

Test Flight With Mock Solar Panel	
Flight Time (*min:sec*)	7:55
mAh Consumed	1789
Predicted *mAh* Consumed	1265
Error	41%

From this flight test data, the actual P_{er} for NanSun was found to be 77.4 Watts. Had the solar cells been able to provide the 77.7 Watts that they were specified to provide, NanSun would have been capable of flying purely on solar energy, albeit with nearly zero excess power.

5.4 Solar Powered Flight Test

On December 30, 2006 a full-system solar powered flight test of NanSun was initiated on a sunny day in Whittier, California. The flight test lasted a mere 37 seconds before suffering a crash that destroyed the plane. The crash was attributed to the omission of a preflight assembly step to secure the wings from rolling on the fuselage during flight. NanSun was not airborne long enough to gather any useful data for finding the energy captured by the tracking solar panel during flight.

Despite its short length, this flight test was useful in that it proved the entire system was capable of operating while airborne. The solar panel was visually confirmed to be moving to face the sun, and it stopped moving once it was facing the sun. Figure 5.8 shows NanSun in a flight path perpendicular to the sun's rays. This image was captured shortly after a turn, and NanSun's solar panel can be seen repositioning itself to face the sun.

This flight test also proved that the UAV could be easily controlled regardless of the tracking solar panel's movement or angular position. One of the turns during this flight test was executed while the solar panel was in a near vertical position. This turn was performed with no noted difference in response compared to the battery powered flight test. However, both the battery powered flight test and this solar powered flight test were conducted in low wind conditions. Crosswinds would likely have affected the UAV's flight and turn response, especially when the solar panel was in a near vertical position.

Fig. 5.8 NanSun flying during the solar powered flight test

5.5 Analysis of Results

Testing of the solar panel revealed that it was capable of capturing 48.5% of the energy it was predicted to capture, and the battery powered flight test revealed that NanSun's analytical model under predicted the UAV's power requirements by 41%.

Even with less solar energy available and more P_{er} than predicted, onboard solar tracking on NanSun would still be advantageous.

By adding the solar tracking components, the UAV suffered a 16.8% increase in P_{er} as described in Section 4.3. Equivalently, by removing the solar tracking components, the UAV would experience a 14.4% decrease in P_{er}. Based on NanSun's actual P_{er} of 77.4 W which was found from the battery powered flight test, a 14.4% decrease in P_{er} would translate into a reduction of 11.1 Watts for the non-tracking version of the UAV. This was assumed to be the additional power needed by NanSun to overcome the extra drag contributed by the solar tracking system, and is denoted by P_{add}. This value remains constant for steady level flight.

The calculation of this additional 11.1 watts needed assumed that the 41.4% error in the analytical model's P_{er} prediction was all due to an under-prediction of drag, and that error in drag was distributed evenly over all of NanSun's surfaces. As described earlier in Section 3.3, this error could have stemmed from sources other than an error in the drag model. However, the error was all attributed to drag in the calculation of P_{add} as a worst-case scenario. The solar tracking system with this particular solar panel, including the tracking system's associated drag contribution, would be advantageous onboard NanSun for a specific range of sun altitude angles. This range includes all sun altitude angles where the difference between the solar panel's power if it were tracking, and the solar panel's power if it were fixed horizontally, is greater than P_{add}. This power difference (P_{diff}) is plotted as a function of sun altitude angle (β) in Figure 5.9. Again, β is the angle of the sun up from Earth's horizon. β is zero at sunrise and sunset, and

β is 90° when the sun is directly overhead. The horizontal line in Figure 5.9 represents P_{add}, the 11.1 additional watts needed to overcome the drag from the solar tracking system. This figure also demonstrates that the solar tracking system's advantage increases as the sun's altitude angle decreases. The altitude angle at which the solar tracking NanSun UAV would no longer be advantageous over a conventional fixed PV panel UAV is about 49.5°, as seen in Figure 5.9 where the P_{diff} curve intersects the P_{add} line.

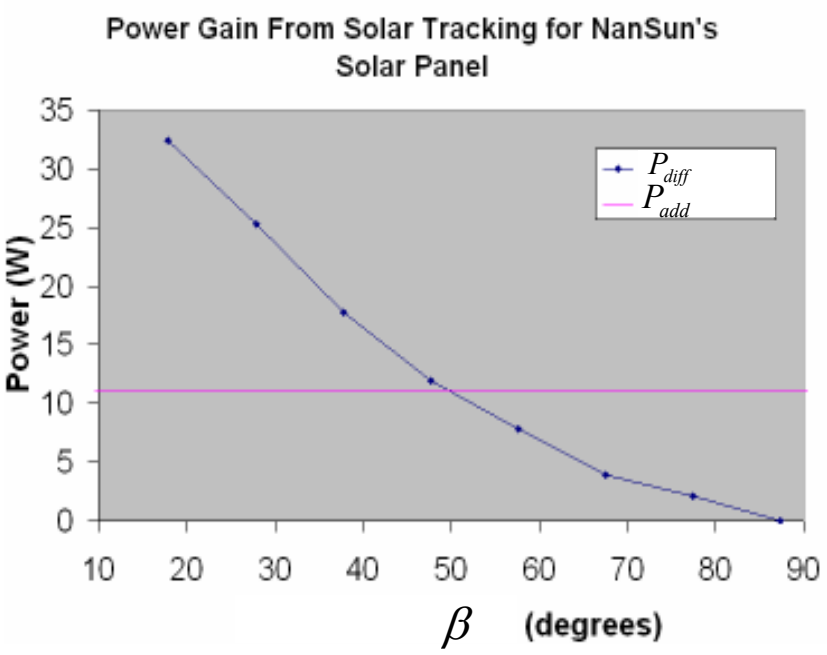

Fig. 5.9 Power gained by NanSun from solar tracking, and additional power required due to excess drag from the solar tracking system

5.6 Global Applications

Using the test data gathered from the solar panel ground test and the battery powered flight test, and with the knowledge the entire system functions while airborne,

some performance predictions could be made for NanSun at different geographical locations and seasons. For NanSun's airframe and solar panel, the power gained by the onboard solar tracker overcomes the power lost due to the solar tracker's drag when the sun's altitude angle is less than 49.5°, as addressed in the previous section. Solar tracking on the NanSun UAV would not be advantageous at times of the day when the sun's altitude angle is greater than 49.5°. However, for long endurance missions, solar tracking on NanSun would still be advantageous if the total energy captured during a mission was greater than the additional energy required for the UAV to overcome the drag of the solar tracking system for that mission. The increase in net energy capture due to onboard solar tracking for a single day (E_{ni}) at any location on the earth can be found by the equation

$$E_{ni} = (P_{\max} - P_{add})T_f - P_{\max}\int_{t1}^{t2} \sin\beta(t)dt\,. \tag{5.2}$$

Again, $P_{\max}$ is the maximum power possible from the solar panel, and $P_{\max}$ occurs when ϕ is zero. T_f is the continuous flight time of the UAV for that day. The last term in this equation represents the power available from an array of horizontally fixed PV cells. Sunrise occurs at time $t1$, and sundown at time $t2$. The sun's altitude angle is expressed as a function of the time of day. For flight missions where E_{ni} is positive, an onboard solar tracking PV panel is advantageous over horizontally fixed PV cells for any solar powered UAV.

Equation (5.2) was solved numerically for NanSun at many of Earth's latitudinal angles in the Northern Hemisphere. Latitude angles north of the Arctic Circle (latitude

66.55° N) were not considered. On the Northern Hemisphere, onboard solar tracking would be least advantageous on the day where β is highest. The β values for the day of June 21 were used at each latitudinal location for this analysis to show the advantage of NanSun's solar tracker on the day that it would be least advantageous.

Significant solar light attenuation from the atmosphere was assumed to occur when β is less than 10^{o}, so the day's length at each latitudinal location was assumed to constitute all of the hours when β was greater than 10^{o}. Mission flight time was also assumed to be equal to the time that the sun's altitude angle was greater than 10^{o}, so T_f was set to be equal to the difference between $t1$ and $t2$. NanSun's predicted net energy gain due to solar tracking is plotted in Figure 5.10 as a function of Earth's latitude angle. The curve was fit to a second order polynomial. This same analysis for Earth's Southern Hemisphere would produce the same curve, except the June 21 data series would occur on December 21.

E_{ni} reaches a minimum at the Tropic of Cancer (latitude 23.45° N), which is the location where β is exactly normal to the Earth's surface at solar noon on June 21. For NanSun, this minimum is near zero by coincidence. In the summertime near the Tropic of Cancer, or in the wintertime near the Tropic of Capricorn, NanSun's solar tracking system as is would not be advantageous over a non-tracking version. The net energy increase of NanSun over a non-tracking version of the UAV would be merely 0.8% near the Tropic of Cancer. If NanSun's solar panel were any less efficient, solar tracking onboard the UAV would actually be a disadvantage near the Tropic of Cancer. The advantage of solar tracking increases as the Earth's latitude angle increases. The net energy increase of NanSun over a non-tracking version of the UAV would be 36% at the

Arctic Circle. The range of latitude angles where NanSun would be significantly advantageous over a non-tracking solar powered UAV appears to lie between about 40^{o} N and 66.55^{o} N, and between 0^{o} and 10^{o} N, as can be seen in Figure 5.10.

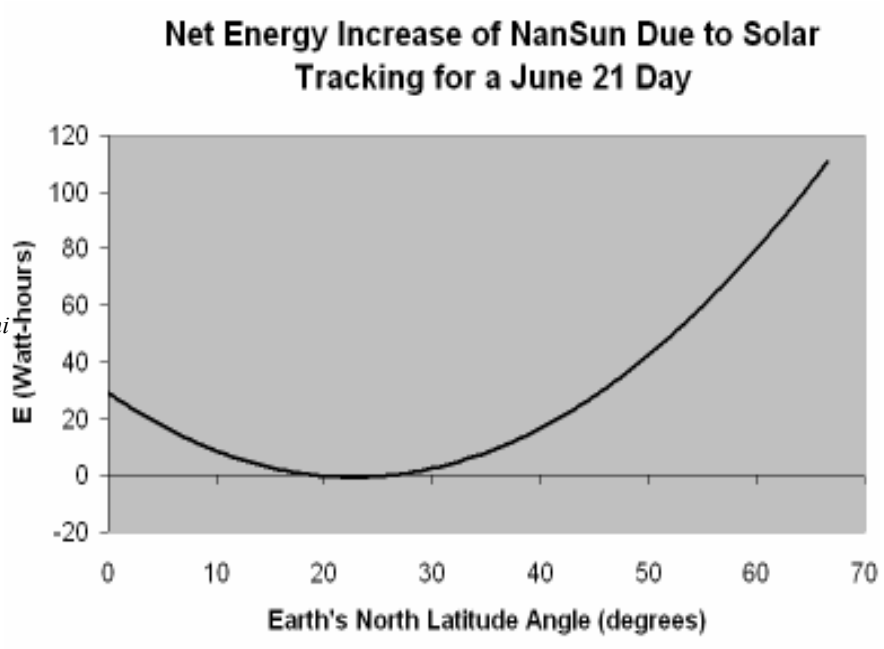

Fig. 5.10 Energy advantage of NanSun's solar tracking system as a function of the Earth's latitude angle, based on the energy available from NanSun's 6.06% efficient PV cells

With more efficient PV cells, NanSun's solar tracking system would be advantageous at any geographical location and any time of year. This is illustrated in Figure 5.11, which represents E_{ni} as a function of latitude angle for NanSun if the PV cells were to provide 51.5% more power, as they were specified to do. In this case, the minimum net energy increase of NanSun over a non-tracking version would be 13% at the Tropic of Cancer, and the maximum net energy increase would be 63% at the Arctic Circle.

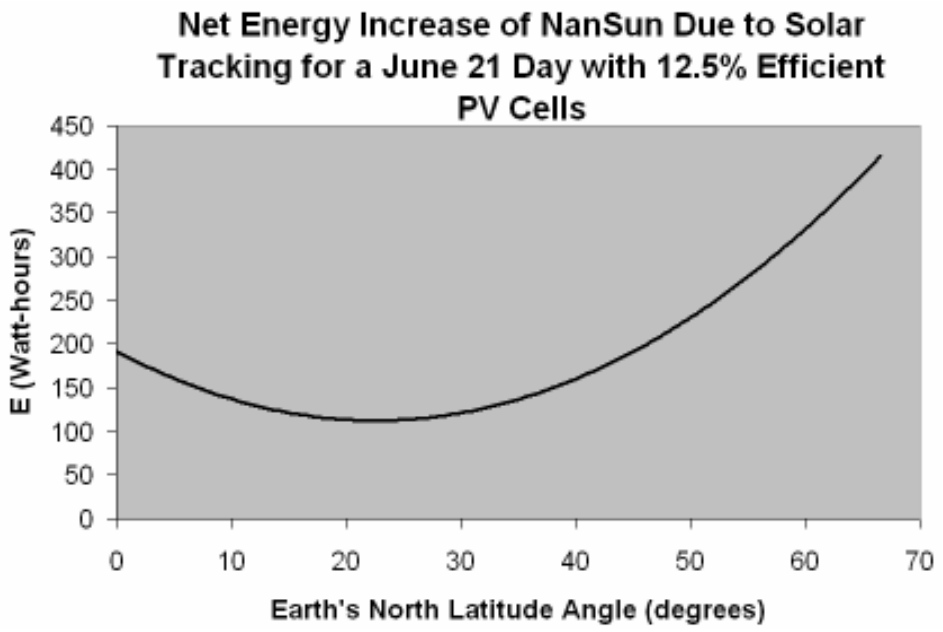

Fig. 5.11 Energy advantage of NanSun's solar tracking system as a function of the Earth's latitude angle, based on the energy available from 12.5% efficient PV cells

Although NanSun's solar panel captured less energy than predicted and the UAV had to be retired without a solar powered long endurance mission, enough data was gathered to draw some useful conclusions.

Chapter 6

Conclusions

6.1 Process Summary

This work has developed a reliable design method for a solar powered UAV with a single axis, onboard solar tracking system. This design method was used to create a series of parametric design spreadsheets for the development of a novel solar powered UAV that allows for more energy capture than conventional solar powered UAVs. This analytical model was optimized to minimize the power required for steady level flight.

A UAV called NanSun was constructed from this design. A solar tracking system was designed for use onboard the UAV. A microcontroller was programmed to control the positioning of the UAV's solar panel to face the sun and track it. The solar tracker system was constructed. An increase in energy capture from solar tracking over a horizontally fixed solar panel was verified with ground tests. A battery powered flight test that lasted 7 minutes and 55 seconds was performed to validate the analytical model's drag and power predictions for the UAV. A full system solar powered flight test was performed to validate the UAV's functionality and performance. This 37 second long flight test ended prematurely when the UAV's wings rotated about its fuselage, which caused it to crash. The energy benefits and penalties of the solar tracking system were compared to conventional solar powered UAV systems.

6.2 Conclusions

The actual P_{er} of the UAV system was found to be 41.4% greater than the analytical design had predicted. The PV cells on the solar panel were found to capture 48.5% of the energy that they were specified to capture. The power penalty for housing the solar tracking system was computed to be 16.8% for the UAV. This power penalty compared the actual P_{er} of the UAV as found from flight testing to the predicted P_{er} of the UAV if the solar tracking system were removed and the PV cells were fixed on the wings. The total energy captured by the tracking solar panel for the entire day of November 10, 2006 in Provo, Utah was found to be 42% greater than the energy capture capability of the same solar panel fixed horizontally.

Data from the battery powered flight test and the solar panel ground tests were used to find ranges of latitude angles around the world where the UAV would have a net energy gain over the same solar powered UAV with no onboard solar tracker. These latitude angles ranged from 0^o to 10^o, and from 40^o to 66.55^o. These latitude ranges correspond to both the Northern Hemisphere and the Southern Hemisphere. With the implementation more efficient PV cells of the same weight, the UAV would have an energy advantage at any geographical location and at any time of year.

The design, embodiment, and analysis of the UAV detailed in this thesis have shown that incorporating an onboard solar tracker into a solar powered UAV can have significant energy benefits over a conventional solar powered UAV with no solar tracker. The onboard solar tracking system described in this thesis also comes with certain detriments. The detriments include a more complex system with more moving parts, and potential adverse flight conditions in strong wind conditions.

The flight tests of NanSun demonstrated that the onboard solar tracking system described in this thesis could successfully be integrated into a solar powered UAV. The methods used in the design of NanSun can be a valuable tool for designing future solar powered UAVs. These methods can be used to determine whether or not developing an onboard solar tracking UAV would be advantageous for any particular solar powered UAV application.

Bibliography

[1] Boucher, R. J., "History of Solar Flight", *20th Joint Propulsion Conference*, Cincinnati, Ohio, June 11-13, 1984, AIAA-84-1429

[2] NASA Facts, "Solar Powered Research", *Dryden Flight Research Center*, Edwards, California 93523

[3] Bowman, W. J., Roberts, C., and Vaughan, M., "Development of a Solar Powered Micro Air Vehicle", *40th AIAA Aerospace Sciences Meeting and Exhibit*, Reno, Nevada, January 2002, AIAA-2002-0703

[4] Berger, B., "NASA Studies Options Following Loss of Helios Vehicle", *Space News*, July 14, 2003, http://www.space.com/spacenews/archive03/nasaarch_071403.html

[5] AC Propulsion, "AC Propulsion's Solar Electric Powered SoLong UAV", 2004, http://www.acpropulsion.com/ACP_PDFs/ACP_SoLong_UAV_48hr_Flight_2005-06-05.pdf

[6] US Naval Observatory Website, *Sun or Moon Altitude/Azimuth Angle Calculator*, http://aa.usno.navy.mil/data/docs/AltAz.html

[7] Raymer, D. P., *Aircraft Design: A Conceptual Approach, Third Edition, AIAA Education Series*, Reston, Virginia, 1999

[8] Bowman, W. J. and Snyder, D., "A Less Minimalist Approach to Teaching Aircraft Design", *44th AIAA Aerospace Sciences Meeting and Exhibit*, Reno, Nevada, January 2005, AIAA-2005-343

[9] Eppler, R., *Airfoil Design and Data*, Springer-Verlag Berlin, Heidelberg, 1990

[10] Simons, M., *Model Aircraft Aerodynamics, Fourth Edition*, Great Brittan, 1999

[11] Foster, T. and Bowman, W. J., "Dynamic Stability and Handling Qualities of Small Unmanned Aerial Vehicles," *43rd AIAA Aerospace Sciences Meeting and Exhibit*, Reno, Nevada, January 2005, AIAA-2006-1023

[12] Hoerner, S., *Fluid-Dynamic Drag*, Midland Park, New Jersey, 1965

Appendix A.

Tracker Controller Code

This appendix contains the PicBasic Pro code that was programmed into the PIC16F877A microcontroller on the UAV's tracker controller board. This code was developed to control the Hitec HS-322HD servo, which positioned the UAV's solar panel to track the sun. The author's comments within this code are preceded by a single apostrophe (').

```
'*****************************************************************
'*  Name    : TRACKER 5.PBP                                      *
'*  Author  : Troy Tegeder                                       *
'*  Date    : 9/26/2006                                          *
'*  Version : 5.0                                                *
'*  Notes   : moves servo to track the sun using voltage         *
'*          : comparators                                        *
'*          : Pulse values are set for Hitec HS-322HD Servo      *
'*****************************************************************

' Starts with no signal to servo's ouput pin
LOW PORTC.1

' Inverts direcion of comparator when =1
CMCON.4 = 0

' Sets comparator register to two independent comparator mode

CMCON.2 = 0
CMCON.1 = 1
CMCON.0 = 0

' Define LCD connections for troubleshooting
DEFINE  LCD_DREG        PORTD
DEFINE  LCD_DBIT        4
DEFINE  LCD_RSREG       PORTE
DEFINE  LCD_RSBIT       0
DEFINE  LCD_EREG        PORTE
DEFINE  LCD_EBIT        1

' Set sensor pins to be inputs
TRISA = %00001011
ADCON1 = 4

' LCD R/W low = write
LOW PORTE.2
' Wait for LCD to startup
PAUSE 500

' don't wait more than 25000 microseconds to find an input pulse

DEFINE PULSIN_MAX 2500

pos         VAR     WORD        ' Servo position
r           VAR     BIT         ' 1  direction, right or left
l           VAR     BIT         ' 0  direction, right or left
old_dir     VAR     BIT         ' stores the servo dir from previous
operation
l_count     VAR     WORD        ' counts comparator outputs with the value
l
r_count     VAR     WORD        ' counts comparator outputs with the value
r
i           VAR     WORD        ' loop counter
j           VAR     BYTE        ' anther loop counter
```

```
servo_dir   VAR     BIT         ' l or r, depends on sampling of comp_out
step_size   VAR     BYTE        ' 24us is the resolution with 4MHz crystal
gear_pulse  VAR     WORD        ' pulse from receiver chanel 5
no_pulse    VAR     BYTE        ' makes sure there are many consecutive 0
pulse
                                '  values before going to sleep
comp_out    VAR     CMCON.6     ' Alias comparator output
servo_sig   VAR     PORTC.1     ' Alias servo signal pin
in_pin      VAR     PORTB.7     ' Alias input pulse pin

' Center servo position, 65 steps from 0
GOSUB center

' direction assign
r = 1
l = 0
step_size = 24
no_pulse = 0

' initialize direction on power up
GOSUB dir_find

IF servo_dir = l THEN
    old_dir = l
    ELSE
    old_dir = r
    ENDIF

' Main program loop
main:

        ' sleep after 15 consecutive low pulses
        GOSUB pulse_count
        IF no_pulse > 15 THEN
            GOSUB go_sleep
            ENDIF

        'finds direction to move servo
        GOSUB dir_find

        IF servo_dir != old_dir THEN
                GOSUB rest
                ENDIF

        IF servo_dir = l THEN
                GOSUB left
                ENDIF

        IF servo_dir = r THEN
                GOSUB right
                ENDIF

        GOSUB move
```

```
        ' Do it all forever
        GOTO main

' See if tracking mode is on or off
pulse_count:
        PULSIN in_pin, 1, gear_pulse
        IF gear_pulse < 140 THEN
            no_pulse = no_pulse + 1
            ENDIF
        IF gear_pulse >= 140 THEN
            no_pulse = 0
            ENDIF
        LCDOUT $fe, 1, "Pulse:", #gear_pulse
        RETURN

' moves the servo, waits for update
move:
    ' Start servo pulse
    HIGH servo_sig
    PAUSEUS pos
    ' End servo pulse
    LOW servo_sig
    PAUSE 16
    RETURN

' Move servo left
left:   IF pos <= (95 * step_size) THEN
                pos = pos + 6
                ENDIF
        old_dir = l
        RETURN

' Move servo right
right:
        IF pos >= (34 * step_size) THEN '
                pos = pos - 6
                ENDIF
        old_dir = r
        RETURN

' this loop keeps the servo from moving as long as the comparator shows a
' change in direction small% of the time, small ms pause time.  The signal
' tolerance is defined as only 1 direction change is allowed out of 2000
' samples.
rest:
        l_count = 0
        r_count = 0
        FOR i = 0 TO 2000
            IF comp_out = 1 THEN
                l_count = l_count + 1
                ELSE
                r_count = r_count + 1
                ENDIF
            IF i > 1999 AND ABS(l_count - r_count) < 1999 THEN
```

```
                i = 1
                l_count = 0
                r_count = 0
                GOSUB pulse_count
                IF no_pulse > 15 THEN
                    GOSUB go_sleep
                    ENDIF
                ENDIF
            ' 400ns needed to restart comparators
            PAUSEUS 24
            NEXT i
        GOSUB dir_find
        GOSUB move
        IF servo_dir = l THEN
            old_dir = l
            ELSE
            old_dir = r
            ENDIF
        RETURN

' samples comparator output
dir_find:


            IF comp_out = 1 THEN
                servo_dir = l
                ELSE
                servo_dir = r
                ENDIF
        RETURN

center:
    FOR i = 1 TO 30
        pos = 1560
        ' Start servo pulse
        HIGH servo_sig
        PAUSEUS pos
        ' End servo pulse
        LOW servo_sig
        PAUSE 16
        NEXT i
    RETURN

' puts microcontroller in low power mode if tracker signal is within
tolerance
go_sleep:
        GOSUB center
        no_pulse = 0
        FOR j = 1 TO 25
            ' Low power pause for about .018 seconds
            NAP 0
            GOSUB pulse_count
            ' stays asleep while 10/25 pulses-low
            IF no_pulse > 10 THEN
```

```
            no_pulse = 0
            j = 1
            GOSUB center
            ENDIF
        NEXT j
        RETURN

END
```